Description and Evaluation of an Emission-Driven and Fully Coupled Methane Cycle in UKESM1

G A Folberth, Z. Staniaszek, A T Archibald, N. Gedney, P. Griffiths, C D Jones, F M O'connor, R J Parker, A A Sellar, A. Wiltshire

JAMES | Journal of Advances in Modeling Earth Systems

RESEARCH ARTICLE
10.1029/2021MS002982

Description and Evaluation of an Emission-Driven and Fully Coupled Methane Cycle in UKESM1

G. A. Folberth[1], Z. Staniaszek[2], A. T. Archibald[2,3], N. Gedney[4], P. T. Griffiths[2,3], C. D. Jones[1], F. M. O'Connor[1], R. J. Parker[5,6], A. A. Sellar[1], and A. Wiltshire[1]

[1]Met Office Hadley Centre, Exeter, UK, [2]Department of Chemistry, University of Cambridge, Cambridge, UK, [3]NCAS-Climate, University of Cambridge, Cambridge, UK, [4]Met Office Hadley Centre, Joint Centre for Hydrometeorological Research, Wallingford, UK, [5]Earth Observation Science, School of Physics and Astronomy, University of Leicester, Leicester, UK, [6]National Centre for Earth Observation, Space Park Leicester, University of Leicester, Leicester, UK

Key Points:

- A methane emission-driven configuration of the UK community Earth system model UKESM1, UKESM1-ems, has been developed
- In UKESM1-ems global wetlands are interactively coupled to the atmosphere at every timestep via methane emissions
- The UKESM1-ems performs well simulating the global methane cycle including feedbacks; the global budget compares well with observations

Correspondence to:
G. A. Folberth,
gerd.folberth@metoffice.gov.uk

Citation:
Folberth, G. A., Staniaszek, Z., Archibald, A. T., Gedney, N., Griffiths, P. T., Jones, C. D., et al. (2022). Description and evaluation of an emission-driven and fully coupled methane cycle in UKESM1. *Journal of Advances in Modeling Earth Systems*, *14*, e2021MS002982. https://doi.org/10.1029/2021MS002982

Received 10 JAN 2022
Accepted 27 JUN 2022

Abstract Methane (CH_4) is one of the most important trace gases in the atmosphere owing to its role as an exceedingly effective greenhouse gas and atmospheric pollutant. Better understanding of the global methane cycle and its interactions with the Earth system is therefore necessary for robust future projections of anthropogenic climate change and assessments of multi-gas mitigation strategies. Here we present a newly developed methane emission-driven Earth system model to simulate the global methane cycle fully interactively. We provide an evaluation of methane sources and sinks and a full-cycle methane budget and its change over the historic period. We further evaluate the methane atmospheric abundance and lifetime against available observations. The new methane emission-driven model simulates all the components of the methane cycle within observational uncertainty. We calculate a total present-day (2000–2009 decadal average) methane source of 591 Tg(CH_4) yr^{-1} with 197 Tg(CH_4) yr^{-1} coming from wetlands. These sources are nearly balanced by the global methane sinks amounting to 580 Tg (CH_4) yr^{-1}; reaction of methane with the hydroxyl radical in the troposphere alone removes 525 Tg(CH_4) yr^{-1}. The imbalance between sources and sinks of 11 Tg(CH_4) yr^{-1} represents the atmospheric methane growth rate and is in fairly good agreement with current best estimates of 5.8 Tg(CH_4) yr^{-1} with a range of 4.9–6.6 Tg(CH_4) yr^{-1}. At present-day the model shows a maximum systematic negative-bias of approximately 200 ppb in the methane surface mole fraction.

Plain Language Summary Methane is a very important greenhouse gas. The global methane cycle needs to be understood fully to accurately model the way methane affects climate change. We describe a new version of the UKESM1 Earth system model, UKESM1-ems, that uses emissions of methane to drive the atmospheric chemistry. In case of emissions from global wetlands, such as bogs, swamps and tundra, the methane emissions are calculated by the model during runtime. Methane emissions react directly to changes in the modeled climate. UKESM1-ems simulates the global cycle of methane from emissions via oxidation in the atmosphere to uptake at the surface more realistically. We also test the model against measurements from satellites and ground-based stations to ensure the relevant processes in the model behave accurately. The comparison with observations shows that UKESM1-ems performs well and represents an improvement in simulating important processes in climate and the Earth system. However, we also found that the methane concentration in the model is too low compared to observations for the period of the twentieth and early 21st century during which human activity, especially the use of fossil fuel, is dominating the methane cycle.

1. Introduction

Methane (CH_4) is the second most important anthropogenic greenhouse gas (GHG), second only to CO_2. Methane's direct radiative forcing accounts for 25% of the anthropogenic radiative forcing since pre-industrial times (Ganesan et al., 2019), adding 0.54 ± 0.11 W m^{-2} (1750–2019) to the total anthropogenic forcing (Forster et al., 2021). The importance of methane as a GHG derives from its large global warming potential (GWP) which exceeds that of CO_2 by a factor of 29.8 ± 11 (Forster et al., 2021) for methane from fossil fuel sources over a 100-year period (GWP-100), while its present-day atmospheric mole fraction is still two orders of magnitude smaller than that of CO_2 (Dlugokencky & Tans, 2020; Dlugokencky et al., 2021). Methane also plays a critical role in atmospheric composition. As a precursor to tropospheric ozone, it contributes significantly to atmospheric

pollution with harmful effects for human and ecosystem health on a global scale (von Schneidemesser and Monks, 2013; von Schneidemesser et al., 2015).

The abundance of methane in the atmosphere is determined by a complex balance of natural and anthropogenic processes, all of which have large uncertainties. Sources of methane include natural processes such as emission of methane from wetlands, ecosystem fires, and termites. Another potentially very large source of methane from natural environments, that could even rival global wetland methane emissions in magnitude, has been reported by Bastviken et al. (2011) and Rosenterter et al. (2021). This methane source originates from inland freshwater systems, such as lakes, reservoirs, ponds, streams, and rivers.

Fossil fuel production, enteric fermentation in ruminant animals, rice cultivation and emissions from landfills make up most of the anthropogenic methane sources. These emissions are estimated to amount to around 334 (321–358) Tg CH_4 yr^{-1} (Saunois et al., 2016, 2020); natural emissions are estimated at 215 (176–243) and 369 (245–485) Tg CH_4 yr^{-1}, respectively, based on a top-down and bottom-up approach for the period 2000–2009 (Saunois et al., 2020).

The atmospheric methane burden has undergone substantial changes over the course of the Earth's history (Quiquet et al., 2015). Methane surface mole fractions have steadily increased since the pre-industrial because of the industrialization of manufacturing and agriculture. Ice core records reveal the onset of an increase in atmospheric methane mole fractions since 1720 attributed to human activity. In 1750 the CH_4 mole fraction in the lower atmosphere had reached 710 ppb (Rubino et al., 2019), increasing roughly by a factor of 2.5–1884 ppb at the end of 2020, based on in situ measurements (Dlugokencky et al., 2021). The dominant contribution responsible for this increase comes from fossil fuel use, livestock, and rice cultivation (Kirschke et al., 2013).

To date, Earth system models, in most cases, have specified atmospheric methane mole fractions to follow prescribed pathways (Eyring et al., 2016) thereby disallowing important coupling mechanisms, in particular coupling between global wetlands and atmospheric chemistry. For instance, during the Coupled Model Intercomparison Project–Phase 5 (CMIP5) most modeling groups, in their submissions to ACCMIP (Atmospheric Chemistry and Climate Model Intercomparison Project; Lamarque et al., 2013), used prescribed methane concentrations throughout the whole atmosphere or at least at the surface level (cf., Table A1, Voulgarakis et al., 2013). In all models contributing to AerChemMIP (Aerosols and Chemistry Model Intercomparison Project; Collins et al., 2017) during CMIP6 global mean methane concentrations were prescribed at the surface (cf., e.g., Griffith et al., 2021), except for some future simulations with GISS-E2-1-G, the NASA Goddard Institute for Space Studies chemistry–climate model version E2.1(Nazarenko et al., 2022), which used interactive online methane emissions.

There have been other previous studies, however, that applied methane emissions to drive the model methane cycle. For instance, LMDzORINCA used anthropogenic emissions from Lamarque et al. (2010) and fixed present day natural emissions of methane during CMIP5 (Szopa et al., 2013). Going a step further, the GISS Model E2 included an interactive wetland methane emission source in addition to prescribed emissions from anthropogenic and biomass burning sources (Shindell et al., 2013). HadGEM2-ES (Hadley Center Global Environment Model–Earth System configuration; Collins et al., 2011; Jones et al., 2011) has also been used in a methane emission-driven configuration for one study (Hopcroft et al., 2017). Heimann et al. (2020) have examined the present-day and future atmospheric methane burden with a methane emission-driven chemistry-climate model. However, until very recently these examples largely remain the exception.

Here, we present a description and evaluation of a methane emission-driven Earth system model that is based on the United Kingdom Earth System Model release version 1.0 (Sellar at al., 2019, 2020; Archibald et al., 2020; Mulcahy et al., 2020), hereafter called UKESM1. UKESM1 has been applied extensively in the Coupled Model Intercomparison Project Phase 6 (CMIP6; Eyring et al., 2016).

The release version of UKESM1 has been modified substantially to run in fully coupled methane emission-driven mode. The new model configuration, denoted as the "emission-driven UKESM1 configuration" or "UKESM1-ems" for short, provides the tool to study the hitherto neglected feedbacks in the global methane cycle. We distinguish between the two configurations by referring to the standard UKESM1 configuration, which is constrained at the surface by methane surface mole fractions, as "concentration-driven UKESM1 configuration" or "UKESM1-conc" for short. Figure 1 summarizes the global methane cycle as it is represented in

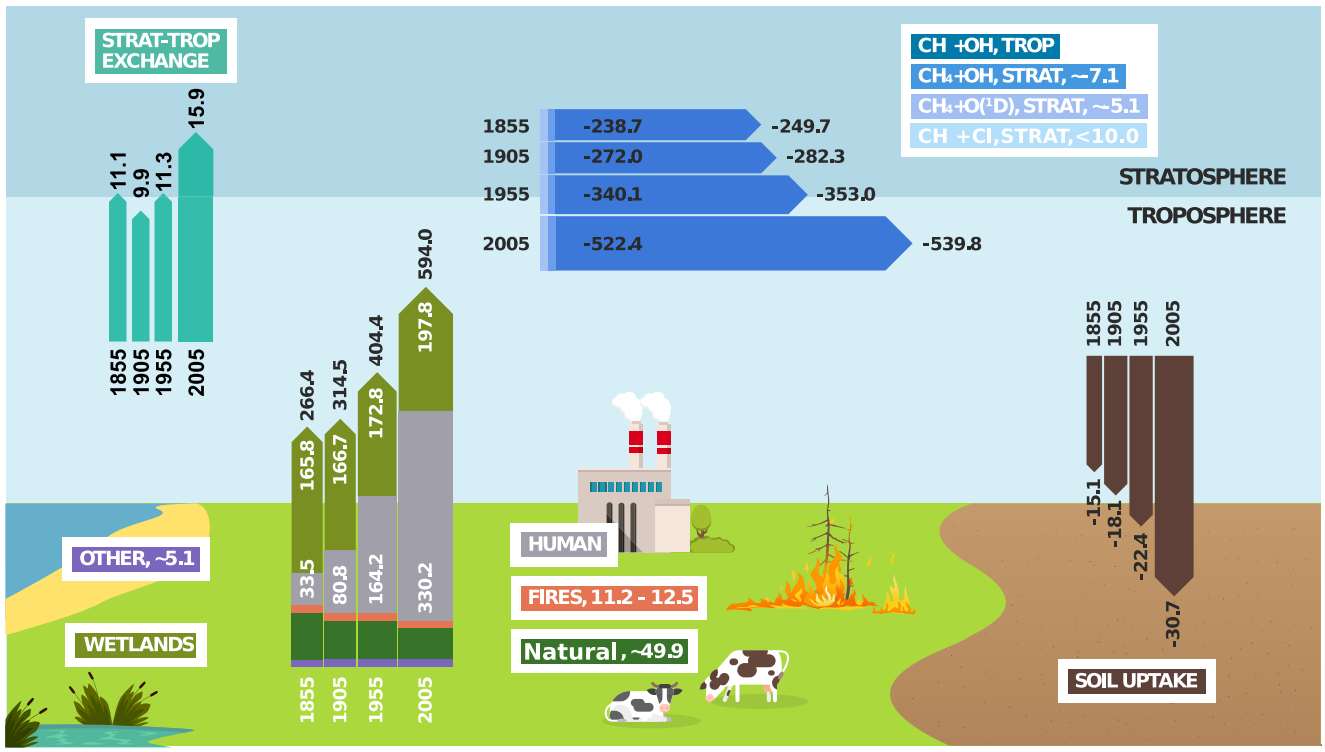

Figure 1. Decadal global mean full-cycle methane budget for the historic period (1850–2014) as represented in UKESM1-ems. The individual budget terms have been calculated with UKESM1-ems and are shown at 50-year intervals. Numbers represent decadal averages of global annual means around the center year indicated in each case. The figure is limited to the dominant fluxes in the global methane cycle as represented in UKESM1-ems.

UKESM1-ems. We only include the dominant budget terms from the historic simulation (1850–2014) in 50-year intervals. Numbers in Figure 1 represent decadal averages of global annual means.

The paper is structured as follows: In Section 2 we summarize the principal components of UKESM1 common to both configurations and describe the required changes applied to UKESM1 to run the CH_4 emission-driven experiment. Section 3 presents an evaluation of the model performance of UKESM1-ems in comparison to UKESM1-conc and to observations of the global methane cycle. In the concluding section we discuss our findings and present directions for future research.

2. Model Description

In this section we briefly describe UKESM1 in its default release configuration (UKESM1-conc) which participated in CMIP6. UKESM1-conc has then been modified to run in methane emission-driven configuration. Nearly all modifications pertain to the atmospheric chemistry and aerosol module UKCA (United Kingdom Chemistry and Aerosol model; Archibald et al., 2020) in UKESM1-conc and comprise updates of the deposition scheme, coupling between UKCA and the Joint UK Land Environment Simulator (JULES), particularly the methane emissions from the wetlands scheme in JULES, and the diagnostic section. In the following we will discuss each of the modifications in more detail.

2.1. The Parent Model UKESM1

The United Kingdom Earth System Model, release version 1.0 (UKESM1), is a fully coupled Earth system model built upon the Met Office coupled climate model HadGEM3-GC3.1 (Hadley Center Global Environment Model Version 3, Global Coupled Model configuration Version 3.1) as the physical core (Kuhlbrodt et al., 2018; Williams et al., 2018). On top of HadGEM3-GC3.1 several component models are built into UKESM1: UKCA representing atmospheric composition (Archibald et al., 2020; Mulcahy et al., 2020), the JULES land surface model simulating terrestrial biogeochemistry and dynamic vegetation (Clark et al., 2011; Harper et al., 2016, 2018),

and MEDUSA (Model of Ecosystem Dynamics, nutrient Utilisation, Sequestration and Acidification), a dynamic ocean biogeochemistry model (Yool et al., 2013). Table 1 of Sellar et al. (2019) presents a list of the coupled interactions between Earth system components included in the release configuration of UKESM1. A more detailed description and evaluation of the model is provided in Sellar et al. (2019, 2020).

We use the same UKESM1 configuration that has been applied for the UK's contribution to the CMIP6 Diagnostic, Evaluation and Characterization of Klima, DECK (Eyring et al., 2016), historical, and ScenarioMIP (O'Neill et al., 2016) simulations, denoted as UKESM1-conc in this study. Further details of the model setup and forcing implementation are presented in Sellar et al. (2019, 2020) and Archibald et al. (2020).

2.1.1. Trace Gas and Aerosol Emissions in the Default Configuration

UKESM1-conc uses both interactive and offline emissions of trace gases and aerosols. However, in the default configuration UKESM1-conc uses prescribed methane concentrations at the surface instead of emission fluxes to constrain the model to scenarios. Furthermore, methane wetland emissions are diagnostic only and methane soil uptake is not considered. For the historic period (1850–2014), offline emissions for anthropogenic trace gases are prescribed with data taken from the Community Emissions Data System (CEDS v2016-07-26, Hoesly et al., 2018; updated to CEDS v2017-05-18 for CO_2 and methane post-publishing) which were prepared for CMIP6 (Eyring et al., 2016). Biomass burning emissions are taken from van Marle et al. (2017). UKESM1-conc interactively simulates emissions of dust, sea salt, primary marine organic aerosols, nitrogen oxide emissions from lightning, and biogenic volatile organic compounds (Archibald et al., 2020; Sellar et al., 2019, 2020).

In UKESM1-conc, the methane cycle is driven via CH_4 surface mole fractions from the CMIP6 forcing data for the historical period described in Meinshausen et al. (2017). Global-mean annual-mean concentrations of methane are prescribed at the surface and methane concentrations evolve freely in all other model levels. The radiation model in UKESM1-conc uses 3D concentrations of methane (as well as O_3 and N_2O) from the UKCA chemistry model, allowing for feedbacks between radiation and atmospheric composition to be simulated. Neither anthropogenic emissions (fossil fuel use, agriculture) nor natural emissions (wetlands, termites, ocean biogeochemistry, hydrates) nor biomass burning sources are accounted for explicitly; CH_4 emissions from the interactive wetland scheme in JULES are purely diagnostic. Methane removal at the surface via soil uptake and microbial decomposition is also not included in the UKESM1-conc default setup.

2.2. Modifications to UKESM1-Conc

The aim of all the modifications was to remove the constraints at the lower boundary by methane surface mole fractions and replace them with methane emissions. We replaced the prescribed surface methane mole fractions with explicit emission sources, included CH_4 surface removal and switched the wetland scheme in JULES from diagnostic to prognostic, thereby coupling the wetland scheme in JULES and the methane photochemistry in the atmospheric composition model UKCA. We will now discuss these model changes in detail.

2.2.1. Natural Sources of Methane

2.2.1.1. Methane Emissions From Wetlands

UKESM1-conc includes an interactive wetland fraction and diagnostic methane emission process model (Clark et al., 2011). However, in UKESM1-conc this wetland methane emission model is used purely diagnostically. The changes made to enable the full methane cycle include the coupling of wetland methane emissions with UKCA. Subgrid wetland extent is calculated interactively with a TOPMODEL based scheme in JULES (Gedney & Cox, 2003; Gedney et al., 2004, 2019). CH_4 production is calculated with a net primary productivity-based substrate parametrization with a hydrogenotrophic methanogenesis pathway, as described in detail in Gedney et al. (2019).

The wetland model is dependent on wetland extent, substrate availability (where used NPP) and temperature, where the temperature response directly follows the Arrhenius equation which described the temperature dependence of a biological process. It does not include some of the more detailed processes, such as CH_4 transport through soil and vegetation and production of CH_4 via different carbon pools. McNorton et al. (2016) demonstrate that including these processes within the standard JULES model does not improve overall performance. Moreover, there is insufficient data to adequately constrain many of these processes (Riley et al., 2011).

The wetland methane emission flux is then added to the atmospheric methane tracer in UKESM1-ems at every timestep, when it becomes subject to atmospheric transport (advection, convection, etc.) and photochemical decomposition in UKCA (Archibald et al., 2020), mainly through reaction with hydroxyl radical. Further details of this coupling are discussed in Hopcroft et al. (2017) and O'Connor et al. (2014).

2.2.1.2. *Other Natural Sources of Methane*

Methane emissions from other important natural sources (termites, oceanic sources, methane hydrates) are not included in the CMIP6 forcing data. In the absence of better understanding, we assume the magnitude of these sources to be constant over the entire period of the simulation (1850–2014). The emissions in each case are based on the work by Fung et al. (1991). Data sets were taken from https://data.giss.nasa.gov/ch4_fung/. CH_4 emissions from oceans and methane hydrates were lumped together and distributed globally using the global distribution of oceanic CO emission from the "Precursors of ozone and their effects in the troposphere", POET, data sets (Granier et al., 2005). The additional global annual total CH_4 source amounts to 49.9 $Tg(CH_4)$ yr^{-1}, with 20.0 $Tg(CH_4)$ yr^{-1} coming from ocean sources, 19.9 $Tg(CH_4)$ yr^{-1} coming from termites, and 10.0 $Tg(CH_4)$ yr^{-1} are assumed to come from methane release from hydrates. The estimates for oceanic sources and hydrates fall within the estimates given in Saunois et al. (2020), albeit on the higher end. Our estimates for termite methane emissions are significantly higher than the current best estimates from Saunois et al. (2020). Our estimates are higher by up to 100% compared to Canadell et al. (2021). Emission of methane from thawing permafrost soils is currently not included in UKESM1-ems. Burke et al. (2017) have developed a new representation of soil carbon for JULES with a specific emphasis on permafrost soils, and this new scheme has been marked for inclusion in the next major release of UKESM. All other natural methane sources are, at this point, considered to be negligible.

Emissions from inland freshwater systems (lakes, ponds, reservoirs, streams, and rivers) could potentially represent a very large global source of methane (Bastviken et al., 2011; Rosenterter et al., 2021). This natural source has been found very sensitive to changes in climate (Tan & Zhuang, 2015; Yvon-Durocher et al., 2014). The emissions seem to be driven mainly by ebullition, which is highly variable in space and time. However, very few process-based models exist at present (Saunois et al., 2020). Furthermore, clearly distinguishing between wetland and freshwater sources in emission inventories can be challenging, rendering global freshwater sources highly uncertain. For these reasons we have not yet included this emission category explicitly in our model.

2.2.2. Pyrogenic and Anthropogenic Methane Sources

We used anthropogenic (CEDS v2016-07-26, Hoesly et al., 2018; CEDS v2017-05-18 for CO_2 and CH_4) and biomass burning (van Marle et al., 2017) methane emission data sets for the historic period (1850–2014). Emissions from fires in forest and grassland ecosystems are still prescribed in UKESM1-ems. However, work is currently in progress to provide these emissions interactively in a future release of UKESM. Methane emissions from natural fires will be provided by INFERNO (INteractive Fire and Emission algoRithm for Natural environments; Mangeon et al., 2016), the fire and emissions model in JULES (Teixeira et al., 2021). Completion of this development is planned for the next major UK Earth System Model release version UKESM2.0.

2.2.3. Photochemical and Physical Methane Sinks

The UKCA stratosphere–troposphere chemistry mechanism (StratTrop version 1.0) included in UKESM1-conc (Archibald et al., 2020) is designed to simulate the O_x, HO_x and NO_x chemical cycles and the oxidation of carbon monoxide, methane, ethane, propane, and isoprene in addition to chlorine and bromine chemistry in the stratosphere. In total the model employs 84 species and represents the chemistry of 81 of these. O_2, N_2 and CO_2 are not treated as chemically active species (Archibald et al., 2020). UKCA StratTrop includes the dominant chemical sinks for methane in the atmosphere. The most important is the reaction of methane with the hydroxyl radical, which is responsible for 80%–90% of the total chemical methane loss (see also Kirschke et al., 2013; Saunois et al., 2020). UKCA StratTrop also accounts for the reaction of methane with excited atomic oxygen radicals, O(1D), which represents an important methane sink in the stratosphere. However, UKCA StratTrop does not include tropospheric halogen photochemistry. In particular, the reaction of methane with chlorine radicals is not accounted for.

Methane removal via soil uptake is not included in the UKESM1-conc. We implemented surface dry deposition for methane in UKCA as described in Archibald et al. (2020) and O'Connor et al. (2014).

2.2.4. Model Calibration and Spin-Up Procedure

With all the modifications to the representation of the methane cycle in UKESM1-ems a systematic drift in the methane concentration between UKESM1-conc and UKESM1-ems must be considered. To assess any such divergent trend between the two configurations, we conducted an initial 30-year simulation with a pre-industrial control setup for UKESM1-ems. A restart-file from the PI-control simulation with UKESM1-conc was used to initialize UKESM1-ems. No divergent trend between the two models could be identified.

Using output from this experiment, we calculate a time series of residual methane surface exchange fluxes for every gridbox location. These residual surface exchange fluxes represent the additional methane source or sink for each gridbox, that would bring UKESM1-ems in complete agreement with UKESM1-conc at every model time-step, with respect to the methane surface mole fraction. We then produced a 2-D, 30-year average monthly mean climatology of residual methane surface exchange fluxes, which represents a bias correction for UKESM1-ems at pre-industrial conditions. The global, annual mean climatological residual methane surface exchange flux amounts to close to 5 $Tg(CH_4)yr^{-1}$ or less than 2% of the total methane emission flux of 266 $Tg(CH_4)\ yr^{-1}$ at pre-industrial conditions. We applied this constant bias correction in all our simulations.

This methane surface exchange flux climatology can be interpreted as the "missing" sources or sinks that are required in our emissions-driven configuration at each gridbox to reproduce exactly the pre-industrial (1850) methane mole fraction in UKESM1-conc. This method of model calibration is referred to as "flux adjustment" (Haney, 1971; Yamazaki et al., 2021). For this procedure it is assumed that UKESM1-conc represents the "true" state with respect to the methane surface mole fraction, since prescribed surface mole fractions are observation-based.

Model spin-up was performed by extending the pre-industrial control simulation to over 300 years after the initial 30 years of test simulation. The transient historic simulations have then been branched off from this pre-industrial control simulations at regular intervals of 40 years each. This procedure produced the three 165-year transient simulations over the historic period (1850–2014).

2.3. Uncertainties in the Global Methane Budget

While methane is one of the key atmospheric constituents due to its role as a potent GHG and major air pollutant, knowledge and understanding of the global methane cycle and budget continues to be incomplete, with large uncertainties still persisting around the main processes. Uncertainties can be grouped into four categories (after Saunois et al., 2020):

1. Uncertainties around methane emitted from wetlands and anthropogenic sources (specifically past emissions)
2. Uncertainties around global methane sinks
3. Uncertainties around regional variation in methane sources/sinks
4. Uncertainties in the modeling of atmospheric transport in the models used in the top-down budget.

Wetland emissions of methane are the largest source of this important atmospheric GHG over the historic period, and they also represent the most important source of uncertainty in the global methane budget (Saunois et al., 2020). Note that another potentially large source of methane with a high degree of variability are emissions from aquatic systems (Rosentreter et al., 2021), but we did not include this source for reason already discussed. Gedney et al. (2019) attribute the main causes of the high level of uncertainty global wetland emissions to: "*a limited knowledge of the present-day wetland extent from observations, and uncertainties in methane emission temperature dependence.*" However, Hmiel et al. (2020) pointed out that estimates of anthropogenic fossil methane emissions may have been substantially underestimated, too, but total anthropogenic methane emissions have rivaled natural sources in magnitude only in the latter half of the twentieth century when this source contributes largely to the overall uncertainty.

Chemical loss of methane, mainly via reaction with the hydroxyl radical in the troposphere, represents another major source of uncertainty (Saunois et al., 2020). The main source of uncertainty from this process comes from inter-model differences in the simulation of OH (Naik et al., 2013; Stevenson et al., 2020; Voulgarakis et al., 2013). Previous studies have attributed the differences in simulated OH to differences in the chemical

Table 1
Comparison of the Global Methane Sources and Sinks, Grouped by Type and Expressed in Tg(CH_4) yr^{-1}, From the UKESM1-Ems Simulation With the Summary From Saunois et al. (2020) and Kirschke et al. (2013) That Provide Bottom-Up (BU) and Top-Down (TD) Estimates

	2000–2009 decadal means in Tg(CH_4) yr^{-1}				
Sources/Sinks	This work	Kir-BU	Kir-TD	Sau-BU	Sau-TD
Sources					
Wetlands	197	217 [177–284]	175 [142–208]	147 [102–179]	180 [153–196]
Anthropogenic	333	331 [304–368]	335 [273–409]	334 [321–358]	332 [312–347]
Wildfires	11	n/a	n/a	3 [1–5][a]	n/a
Termites	20	11 [2–22]	n/a	9 [3–15]	n/a
Oceanic sources	21	18 [2–40]	n/a	13 [9–22]	n/a
Methane hydrates	9	0	n/a	2 [0–5]	n/a
Sinks					
Total chemical loss	549	604 [483–738]	528 [510–538]	595 [489–749]	505 [459–516]
Tropospheric OH	525	528 [454–617]	n/a	553 [476–677]	n/a
Tropospheric O(1D)	1	n/a	n/a	n/a	n/a
Stratospheric OH, O(1D)	23	51 [16–84]	n/a	31 [12–37]	n/a
Tropospheric Cl	n/a	25 [13–37]	n/a	11 [1–35]	n/a
Soil uptake	31	28 [9–47]	32 [26–42]	30 [11–49]	34 [27–41]
Overall Budget					
Sum of sources	591	678 [542–852]	553 [526–569]	703 [500–842]	552 [488–590]
Sum of sinks	580	632 [592–785]	550 [514–560]	625 [500–798]	540 [486–556]
Imbalance	11	n/a	3 [−4–19]	78	3 [−10–38]
Atmospheric growth	9.3	n/a	6	n/a	5.8 [4.9–6.6]

Note. Uncertainties are reported as the [min-max] range of included studies. Differences of up to 1 Tg(CH_4) yr^{-1} in the totals can occur due to rounding errors.
[a]From Saunois et al. (2020).

mechanisms applied in the individual models, varying treatments of the ozone photolysis rate, and modeled ozone and carbon monoxide (cf. Wild et al., 2020; Zhao et al., 2019, Nicely et al., 2018; Szopa et al., 2021).

2.4. Summary of Experiments

For the evaluation of UKESM1-ems we conducted several centennial-scale simulations starting with a 300 years long model integration with constant pre-industrial conditions. This pre-industrial control simulation serves as reference and to produce the methane surface flux adjustment climatology, as described in the previous section. We then produced an initial condition ensemble simulation covering the historical period from 1850 to 2014. The ensemble simulations consist of three simulations spanning 165 years each.

3. Model Evaluation

3.1. The Global Full-Cycle Methane Budget

Methane has several important natural and anthropogenic sources, but only one dominating global sink in the form of reaction with the hydroxyl radical in the troposphere. For an emission-driven model of the global methane cycle it is imperative that these individual sources and sinks, and the processes that drive them, are represented with high accuracy and balance out. The individual components of the methane budget in the model, as summarized in Table 1, are all within estimated uncertainties reported in the literature (Saunois et al., 2020), but their combination does not precisely reproduce the observed increase in methane mole fractions.

Methane from wetlands represents the biggest individual source of methane globally and our interactive simulation of this source is in very good agreement with current estimates. Saunois et al. (2020) report best estimates

ranging from 147 Tg(CH_4) yr^{-1} to 217 Tg(CH_4) yr^{-1} expressed as decadal means over the period 2000–2009 (see Table 1). In UKESM1-ems we calculate a decadal mean wetland methane emission flux of 197 Tg(CH_4) yr^{-1} over the same period. Also, total anthropogenic methane emissions are in good agreement with the best estimates in Saunois et al. (2020), but that is hardly surprising since these emissions are prescribed from ancillaries.

As mentioned above, reaction with hydroxyl radicals in the troposphere is the predominant sink (by far) for atmospheric methane. UKESM1-ems predicts a global decadal mean loss of 525 Tg(CH_4) yr^{-1} from the atmosphere for the period 2000–2009 via this route. Thus, the atmospheric methane sink, interactively calculated with the UKCA-StratTrop mechanism (Archibald et al., 2020) in UKESM1-ems, is in very good agreement with best estimates presented in Saunois et al. (2020) and lies well within the fairly large uncertainty range extending between roughly 450 Tg(CH_4) yr^{-1} and 675 Tg(CH_4) yr^{-1} reported in this meta-study (see Table 1). The interactively calculated methane removal at the surface via uptake by the soil of 31 Tg(CH_4) yr^{-1}, while only a minor sink, also agrees well with best estimates reported in Saunois et al. (2020).

Overall, the calculated total methane source of 591 Tg(CH_4) yr^{-1} and total methane sink of 580 Tg(CH_4) yr^{-1}agrees well with the best estimates in Saunois et al. (2020). The numbers presented here refer to global decadal means over the period 2000–2009, This results in an imbalance between global methane sources and sinks of 11 Tg(CH_4) yr^{-1} in UKESM1-ems which represents the atmospheric methane growth rate. Independently, we calculate a decadal mean methane growth rate of 9.3 Tg(CH_4) yr^{-1} in our model. The difference between growth rate and source-sink-imbalance could be due to numerical errors or potentially non-conservation issues in the transport scheme will have to be investigated further. However, both estimates are in close agreement with the estimates by Saunois et al. (2020) and Kirschke et al. (2013) summarized in Table 1.

3.2. Interactive Wetland Emissions

In our model, methane emissions are calculated interactively at every timestep, based on a global distribution of wetlands provided by JULES, the Joint UK Land Environment Simulator (Best et al., 2011; Clark et al., 2011). Recently, Gedney et al. (2019) presented a comparison of the wetland fraction in the standalone version of the JULES land surface model with observation-based global wetland products. Here, we have evaluated the wetland model in JULES when coupled to the atmosphere in UKESM1-ems, against the Wetland Area and Dynamics for Methane Modeling (WAD2Mv2 Zhang et al., 2021), observation-based product (Figure 2, top row). WAD2M combines a time series of surface inundation based on active and passive microwave remote sensing with six static data sets that discriminate inland waters, agriculture, shoreline, and non-inundated wetlands. In this fully coupled configuration, the wetland scheme shows a similar level of skill as the stand-alone version evaluated in Gedney et al. (2019).

In the mid and high latitudes UKESM1-ems simulates the largest observed wetland regions, although it tends to underestimate their local extent (gridbox wetland fraction). UKESM1-ems also tends to simulate greater regions with small amounts of inundation, which are not evident in the WAD2Mv2 (Zhang et al., 2021) remote sensing product. Similarly, in the tropics, UKESM1-ems simulates the broad patterns well but the local areas with high wetland cover tend to have lower inundation fractions than those in WAD2Mv2. This is particularly true for the Amazon River basin. As the inundation model only includes groundwater and local precipitation flooding and not fluvial flooding (Best et al., 2011), this under-estimate is unsurprising. These differences are also driven by errors in the simulated precipitation, where there is a dry bias over much of Amazonia (Sellar at el., 2019). UKESM1-ems also simulates the general seasonal timings of maximum wetland extent, albeit under-estimating its magnitude (Figure 2, middle and bottom rows).

Model estimates of global annual total methane emissions from wetlands are in very good agreement with other bottom-up and top-down estimates reported in the literature (Kirschke et al., 2013; Saunois et al., 2020). Under present-day conditions (2000–2009 decadal mean) UKESM1-ems calculates a decadal mean annual global total methane emission flux from wetlands of 197 Tg(CH_4) yr^{-1} (Table 1). Bottom-up and top-down best estimates from previous work range between 147 Tg(CH_4) yr^{-1} to 217 Tg(CH_4) yr^{-1}, but the uncertainty in those estimates is much higher (cf., Table 1 and Saunois et al., 2020).

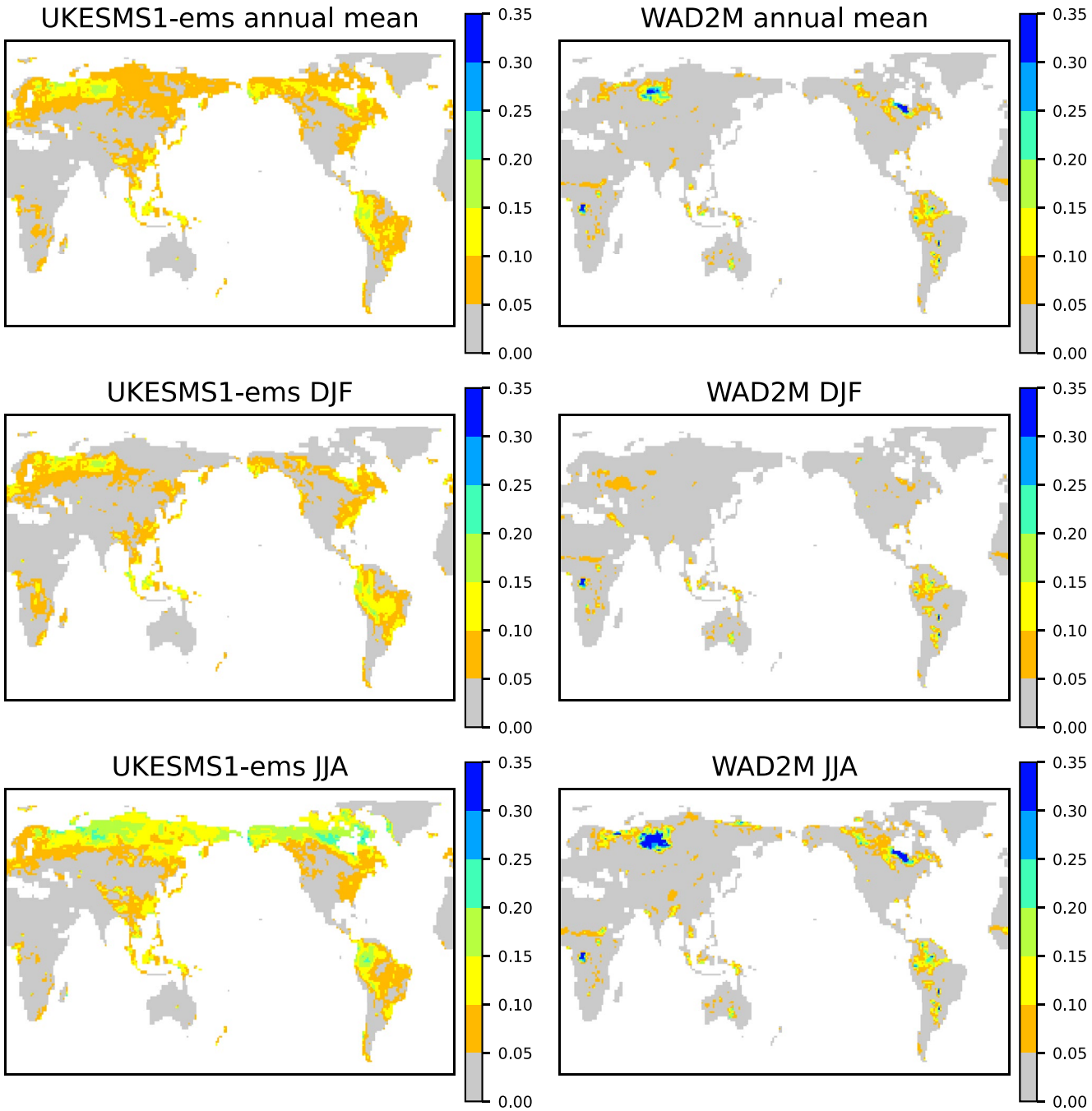

Figure 2. Contemporary wetland fraction. One UKESM1-ems ensemble (left) and WAD2Mv2 (Wetland Area and Dynamics for Methane Modeling; Zhang et al., 2021) product (right). Both are averaged between the years 2000 and 2014. Multi-annual mean (first row), December, January, February mean (second row) and June, July, August mean (third row).

3.3. Global Methane Sinks

3.3.1. OH Distribution and Methane Lifetime

The hydroxyl radical (OH) has a very short chemical lifetime of less than a second and readily reacts with many atmospheric constituents. The atmospheric OH number density is used as a measure for the oxidative capacity of the atmosphere. Reaction with OH is the most important removal process for methane and far outweighs any other methane sink by at least an order of magnitude. However, due to its very short chemical lifetime, direct

measurement of OH in the atmosphere is very challenging. Instead, tropospheric mean OH number densities have commonly been inferred from measurements of trace gases with lifetimes longer than the timescale of tropospheric mixing, whose emission source is well known, and whose primary loss is via reaction with OH.

Recent studies differ on the OH trend over the past decades and into the future. For instance, Nicely et al. (2018) did not identify a significant trend in the tropospheric OH concentration, $[OH]_{trop}$. In their study $[OH]_{trop}$ was derived from methyl chloroform inversions, over the period 1980–2015 which the authors attribute to compensating factors (increasing methane abundance vs. rising tropospheric water vapor, increased nitrogen oxide abundance and rising temperatures). Stevenson et al. (2020) on the other hand, identified a 10% increase in $[OH]_{trop}$ over the same period with an associated decrease in methane lifetime. The authors explain that all models analyzed in the study show similar historic trends in global OH with relative stability between 1850 and 1980, followed by a strong increase in OH by up to 9% between 1980 and 2015. The authors explain that the modeled change in OH, and consequently the methane lifetime, was not inconsistent with OH trends derived from inversions (e.g., Nicely et al., 2018) given the wide uncertainty range.

The findings presented in Stevenson et al. (2020) are based on a multi-model analysis of $[OH]_{trop}$ and methane lifetime data from AerChemMIP (Aerosol and Chemistry Model Intercomparison Project; Collins et al., 2017) experiments for the historic period (1850–2014). Naik et al. (2013), on the other hand, found no significant trend in $[OH]_{trop}$ between the pre-industrial (1850) and present-day (2000) in their multi-model analysis of time-slice experiments conducted during CMIP5 ACCMIP. Our own simulations with UKESM1-ems, shown in Figure 3a, produce an $[OH]_{trop}$ trend similar to that found in Stevenson et al. (2020).

The 1850–2014 trend in the tropospheric OH number densities for UKESM1-conc (solid black line in Figure 3a) and UKESM1-ems (solid red line in Figure 3a) of UKESM1-ems appear to be very close over the entire pre-industrial-to-present-day period: both simulations show an overlapping, almost constant trend from 1850 to about 1980 around 11.5×10^5 cm^{-3} and an 8% rise between 1980 and 2014 to 12.5×10^5 cm^{-3}. A closer examination of the OH trends from the two model configurations reveals, however, that the OH trend in UKESM1-ems after approximately 1950 is discernibly more rapid. This can be seen from the inlay in Figure 3a, which depicts time series of the tropospheric ensemble mean relative OH number density anomalies (with respect to the pre-industrial, 1850–1859 decadal mean OH number density). After 1950, when anthropogenic emissions of methane overtake natural sources in magnitude, the ensemble mean relative OH anomalies are 2%–4% higher in UKESM1-ems (solid red line in the inlay in Figure 3a).

The trends in tropospheric OH number densities are closely related to the trends in the methane atmospheric lifetime (Figure 3b). Methane lifetimes in this study are defined as the *lifetime with respect to removal of methane by OH in the troposphere and calculated as the whole atmosphere methane burden divided by the tropospheric CH_4+OH reaction flux* (cf. Prather et al., 2012). Figure 3b shows that the ensemble mean methane lifetime inUKESM1-ems diverges from that in UKESM1-conc starting around 1950. In 2014 the ensemble mean methane lifetime is approximately 8.2 years, which is two to three months or approximately 3% lower than in UKESM1-conc. The difference between the two configurations with respect to methane lifetimes is relatively small, but significant in the sense that it is bigger than the spread around the ensemble means in both simulations (shaded areas in Figure 3b).

It should also be noted that a present-day (2000–2009 decadal mean) methane lifetime of 8.5 ± 0.1 years in our CH_4-emissions driven simulation is in fairly good agreement with previous modeling studies, albeit on the shorter side of the range: observation-based studies have derived a methane lifetime of 9.8 years for the period 1983–2015 (Nicely et al., 2018), 9.1 ± 0.9 years for the year 2010 (Prather et al., 2012), and $10.2^{+0.9}_{-0.7}$ years for the period 1978–2004 (Prinn et al., 2005). Multi-model ensemble averages of 8.4 ± 0.3 years for the period 2005–2014 (Stevenson et al., 2020), 9.7 ± 1.5 years for the year 2000 (Naik et al., 2013), 10.2 ± 1.7 years for year 2001 (Fiore et al., 2009), and 9.7 ± 1.7 years for the period 1995–2004 (Shindell et al., 2006) have been reported in the literature.

The atmospheric oxidation capacity, measured as the global mean OH abundance in the atmosphere, is sensitive to both the amount of OH and its spatial distribution in the atmosphere (Lawrence et al., 2001; Lelieveld et al., 2016; Naik et al., 2013; Stevenson et al., 2020; Voulgarakis et al., 2013). It is therefore critical to not only accurately simulate the global mean OH concentration but also the distribution of OH throughout the atmosphere.

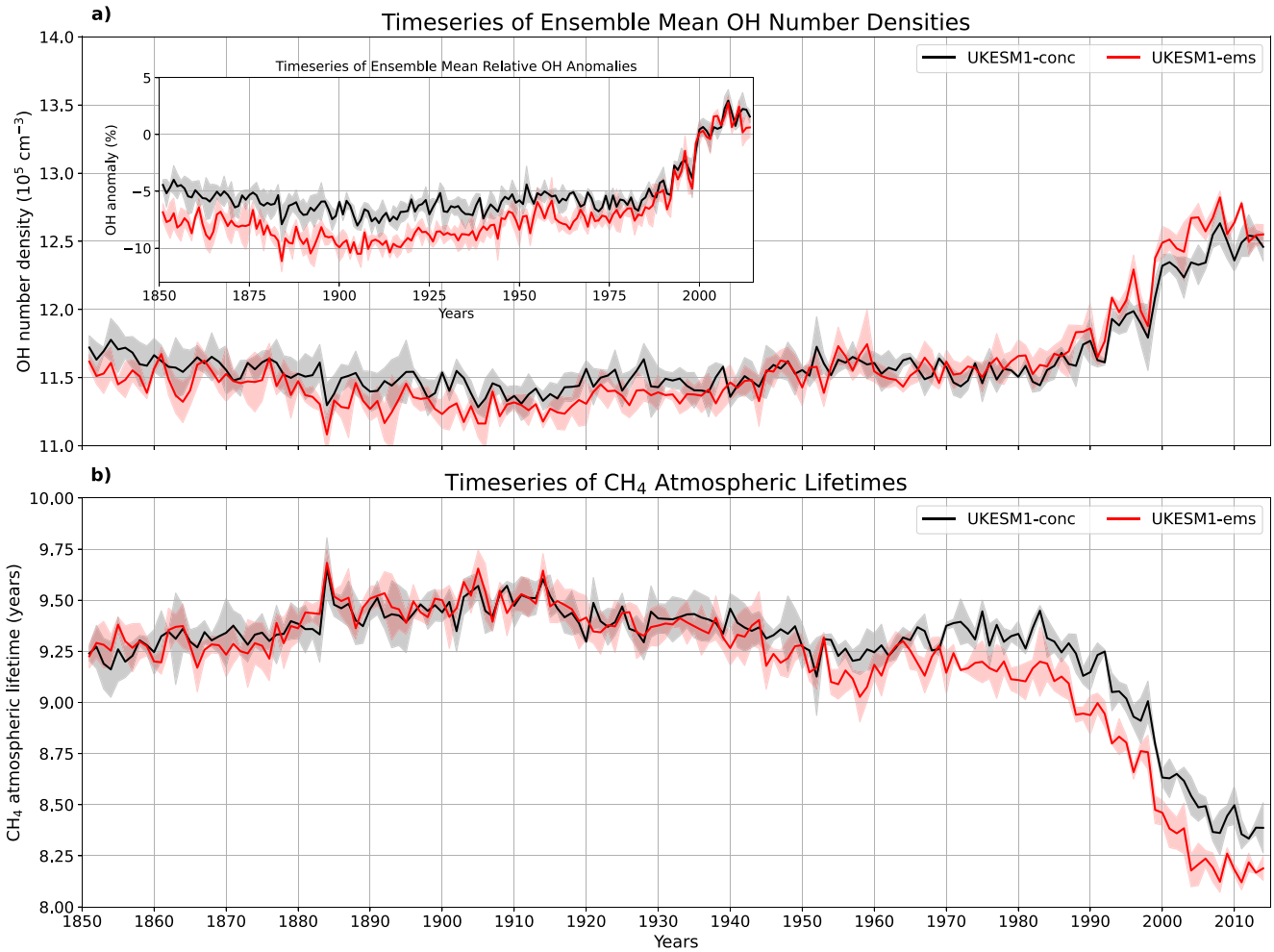

Figure 3. Time series of tropospheric OH number densities and methane lifetimes: (a) 1850–2014 trends in the ensemble mean annual mean OH number densities and (inlay) trends in the ensemble mean annual mean relative OH anomalies with respect to the 1850–1859 decadal mean OH number densities for UKESM1-conc (solid black line) and UKESM1-ems (solid red line), respectively; (b) 1850–2014 trends in the ensemble mean methane lifetime with respect to loss via reaction with OH in the troposphere for UKESM1-conc (solid black line) and UKESM1-ems (solid red line). The shaded areas around the mean trends in each case denote the ensemble spread expressed as the one standard deviation ($1-\sigma$) interval.

In Figure 4 we compare the ensemble mean decadal average regional OH distribution for 12 tropospheric sectors after Lawrence et al. (2001) in UKESM1-ems with previous work.

Consistent with previous studies (Naik et al., 2013; Spivakovsky et al., 2000) OH concentrations are highest in the tropical troposphere between 1000 hPa and 500 hPa. OH concentrations vary nearly fivefold between $22.8 \pm 3.8 \times 10^5$ cm^{-3} in the northern tropical (0°N–30°N) lower troposphere (>750 hPa) and $5.5 \pm 3.3 \times 10^5$ cm^{-3} in the southern extratropical (90°S–30°S) upper troposphere/lower stratosphere (UT/LS) region (500 hPa–250 hPa).The spread in the ensemble mean is relatively large, though, indicating considerable uncertainty around the processes controlling OH in the model.

Generally, our model is in good agreement with previous studies. The model overestimates OH in the tropical lower troposphere. In the other tropospheric regions, our model is in close agreement with the previous studies, particularly with the results from the ACCMIP multi-model means reported in Naik et al. (2013). Figure 4 also shows that UKESM1-ems and UKESM1-conc perform very similarly with respect to simulating OH.

3.3.2. Coupling to Carbon Monoxide

Carbon monoxide (CO) is an intermediate product of methane oxidation, predominantly via reaction with the hydroxyl radical in the troposphere, but also has substantial primary sources from fossil fuel use and biomass

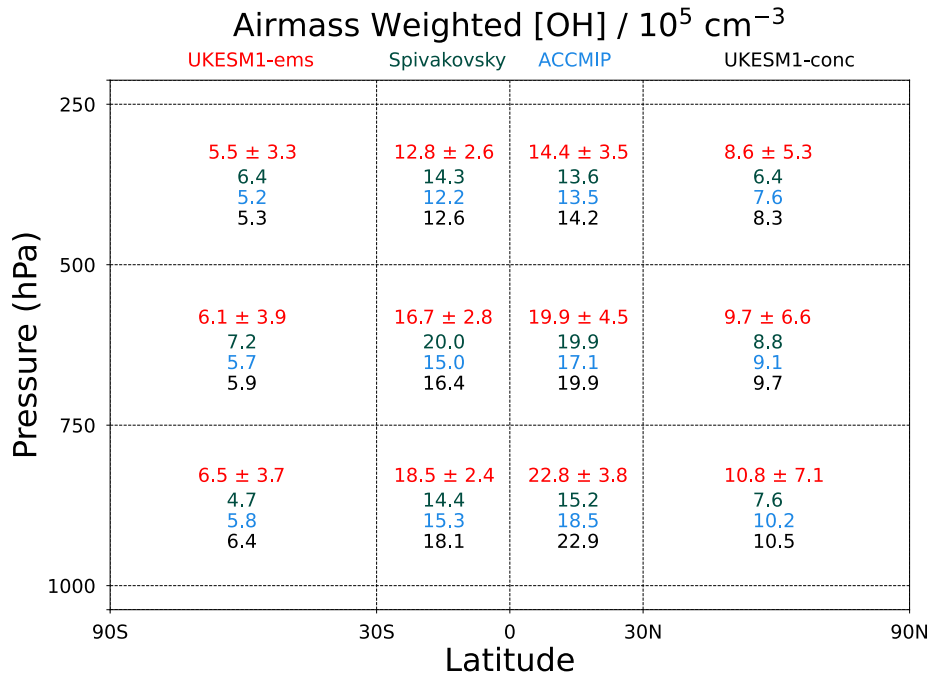

Figure 4. Comparison of decadal average regional annual mean airmass weighted OH concentrations ($\times 10^5$ molecules cm^{-3}) for the period 2000–2009 in 12 tropospheric sectors after Lawrence et al. (2001). The ensemble means and spread, expressed as the standard deviation, for UKESM1-ems in red are compared with the 3D-climatology of OH concentrations from Spivakovsky et al. (2000) in green, results from the multi-model analysis by Naik et al. (2013) in blue. Also included are OH concentrations from UKESM1-conc in black (Archibald et al., 2020).

burning. CO has an atmospheric lifetime of less than 2 months on average. Atmospheric carbon monoxide mole fractions are strongly coupled to methane OH chemistry (Prather, 1994). We compare model output for carbon monoxide from UKESM1-conc and UKESM1-ems with observations of CO surface mole fractions from the NOAA GML (Global Monitoring Laboratory) Carbon Cycle Cooperative Global Air Sampling Network (Dlugokencky et al., 2021) in Figure 5. We evaluate against CO as a second, independent way of assessing the impact of our methane emission-driven setup on the performance of the model with respect to OH.

For the southern hemisphere the latitudinal distribution of carbon monoxide in both model configurations agrees well with the observations. Both model configurations have a high bias in the CO surface mole fraction between approximately 30°S and 20°N suggesting a potential overestimation of CO emissions from biomass burning. The model also has a negative bias between roughly 45°N to 90°N with respect to observed CO surface mole fractions. Many models have reported a similar negative bias in this region (e.g., Naik et al., 2013; Stein et al., 2014; Strode et al., 2015, 2016). Recently, Heimann et al. (2020) showed that increased CO and methane emissions could each at least partially resolve the negative bias in carbon monoxide, but they also argue that the negative bias in CO could be due to missing higher VOC sources. However, without targeted sensitivity experiments it is difficult to conclusively attribute these biases to primary emissions of CO or to secondary in situ CO production from chemical oxidation of methane and non-methane volatile organic compounds (NMVOC) in our model. Such experiments are beyond the scope of this first assessment of the model's performance but will be addressed in a follow-up study.

Figure 5 also shows that UKESM1-ems (red line in Figure 5) is negatively biased with respect to UKESM1-conc. This can be attributed to the negative bias in the methane surface mole fraction in UKESM1-ems (cf. Figure 7). Atmospheric methane mole fractions will be investigated in Section 3.4.

The negative bias in carbon monoxide surface mole fractions relative to the observations at northern mid-to high latitudes persists over the entire period for which observations are available. This can be seen from the time series differences between model and observations shown in Figure 6. The differences between the time series of CO mole fraction anomalies (relative to the CO mole fraction at 90°S) are most pronounced around 45°N

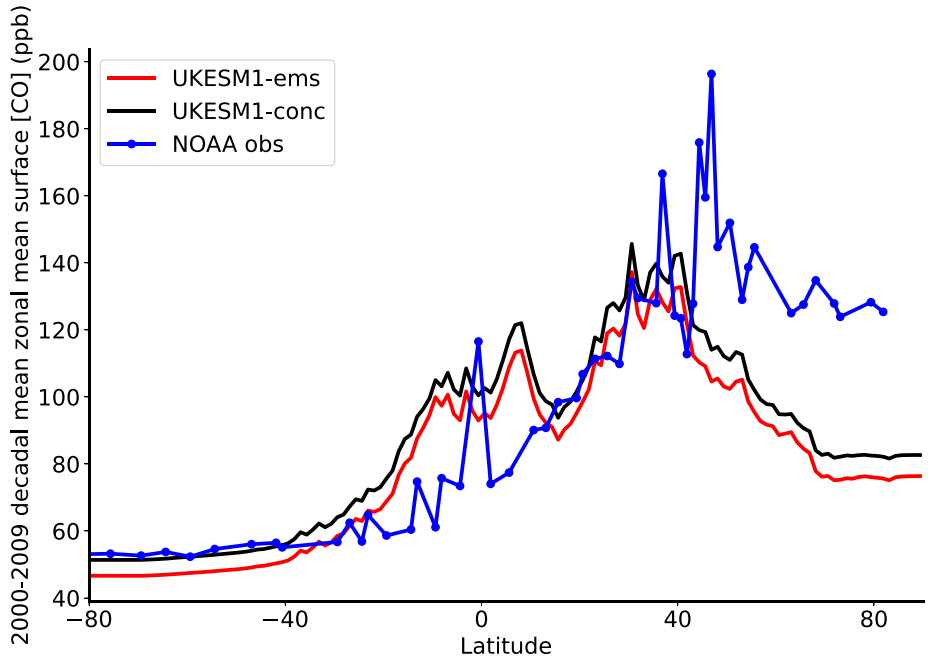

Figure 5. Interhemispheric gradient of decadal mean annual mean carbon monoxide surface mole fractions, averaged over the period 2000–2009, for UKESM1-conc (black) and UKESM1-ems (red), respectively. Model output is compared to observations from the NOAA GML (Global Monitoring Laboratory) Carbon Cycle Cooperative Global Air Sampling Network for carbon monoxide for the same period.

in both configurations of UKESM1, where both model configurations are biased low against the observations. Below 40°N and extending to 30°S both model configurations are overestimating CO surface mole fractions consistently, except for a 10-year period between approximately 1990 and 2000. During this period both model configurations of UKESM1 show a clear negative bias in a narrow region around 20°N and, to a lesser extent, around 10°N. After the year 2000 the bias disappears and re-emerges at the end of the time period (2010–2014).

Attribution of these biases to one process is difficult and is beyond the scope of this study. However, we note that methane surface mole fractions, at least in UKESM1-conc, show very good agreement with observations at most latitudinal zones for which we find biases in carbon monoxide relative to the observations (cf. Figure 10).

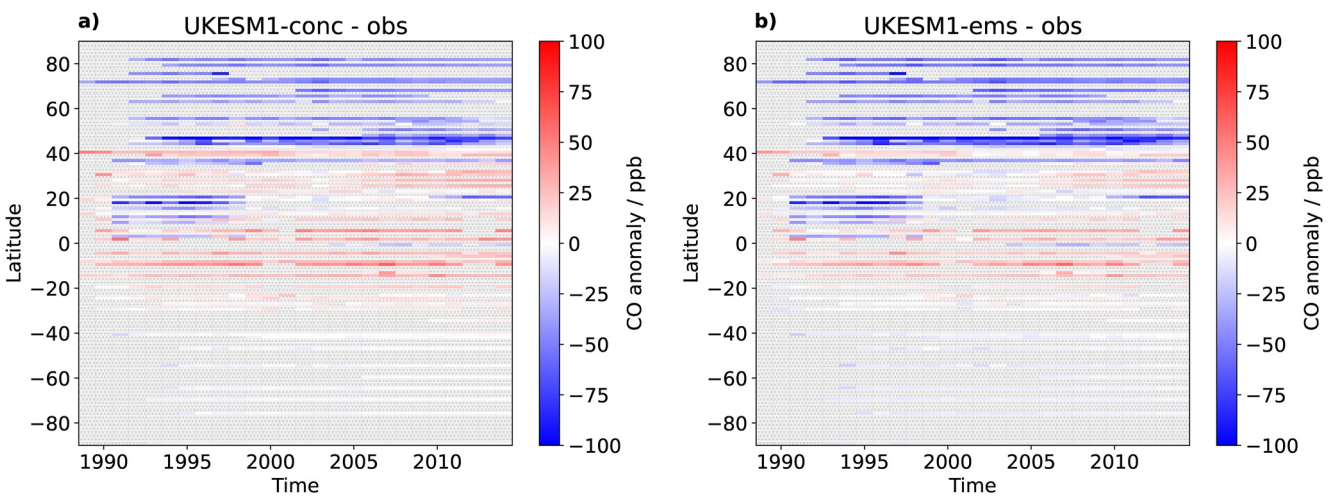

Figure 6. Difference in the time series of the annual zonal mean CO surface mole fraction anomalies (with respect to the CO surface mole fraction at 90°S) for the period 1990–2014 between the simulation with UKESM1 and NOAA GML observations (Dlugokencky et al., 2021) for UKESM1-conc (left plot) and UKESM1-ems (right plot). Gray stippling indicates data points for which no observations are available.

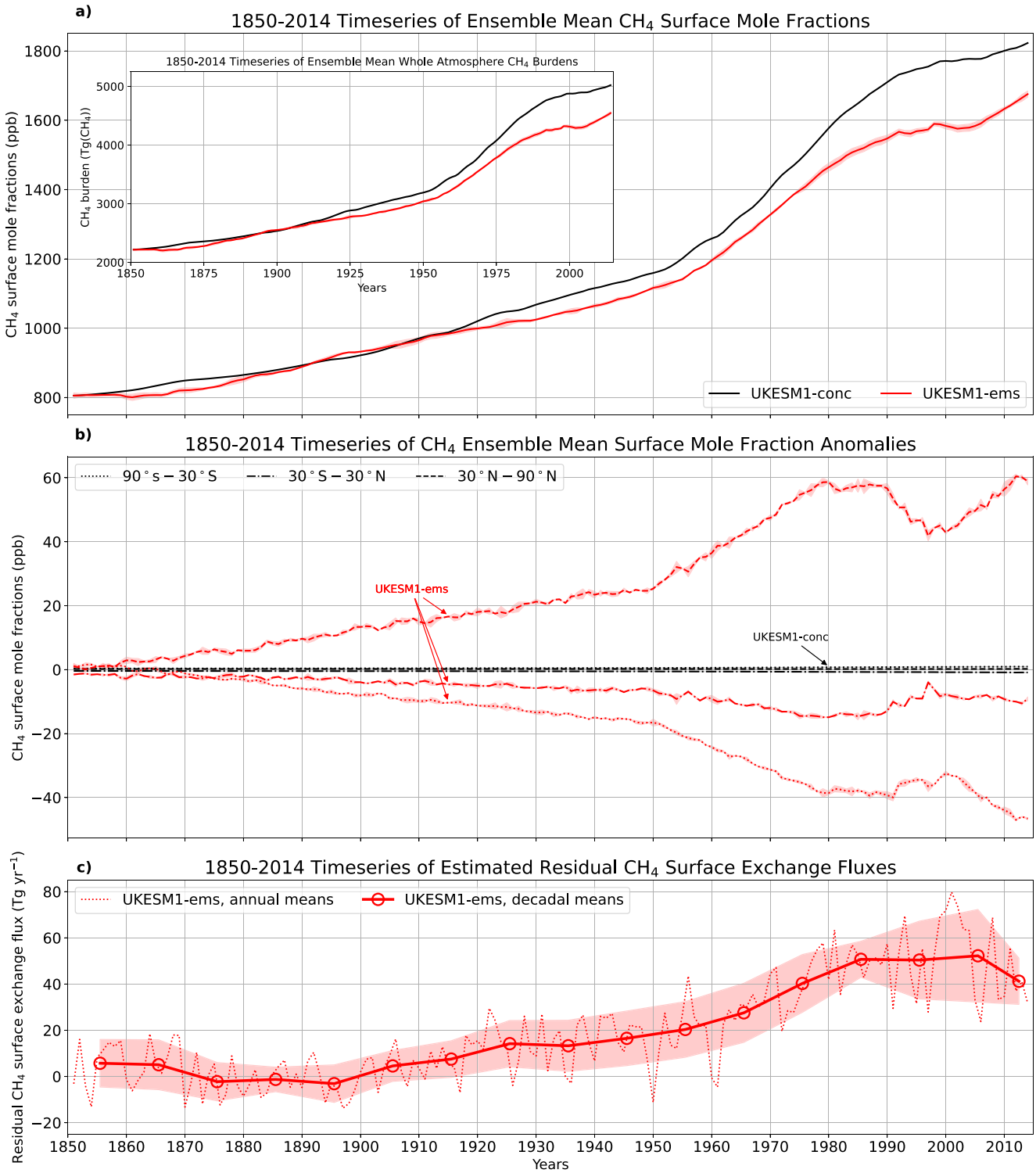

Figure 7.

As we shall discuss later in more detail, methane surface mole fractions are biased low throughout the northern hemisphere in UKESM1-ems. This indicates that the CO biases in the model are not directly attributable to biases in the methane surface mole fractions and may be controlled by other processes in the model independently, such as for instance loss of HO_2 radicals on aerosols (Mao et al., 2013). Further research is required.

3.4. Atmospheric Abundance and Distribution of Methane

The dynamic equilibrium between its sources and sinks determines the atmospheric abundance of methane. In the previous section we have closely examined the simulated CH_4 sources and sinks for two configurations of the UKESM1 Earth system model, one in which methane is constrained by observation-based surface mole fractions at the lower-most model level and one that is driven by methane emissions from the coupled JULES wetland model and methane emission scenarios from CMIP6. In this section we evaluate the resulting methane surface mole fraction and atmospheric burden, based on the simulation over the historical period (1850–2014).

3.4.1. Methane Surface Mole Fractions and Atmospheric Burden

Global annual mean methane surface mole fractions agree very well with those from UKESM1-conc for the first part of the 165-year long simulation as is shown in Figure 7 a. This figure compares atmospheric methane abundances and their evolution in time for the two configurations of UKESM1. Between 1850 and 1920 UKESM1-ems predicts nearly identical methane surface mole fractions as UKESM1-conc, but the latter is constrained at the surface by methane observations. Hence, the global mean surface mole fractions in UKESM1-conc are equivalent to observed values over the period shown.

After 1920 the time series of global annual mean surface mole fractions diverge between the two model configurations. The negative bias in UKESM1-ems reaches a maximum difference of approximately −200 ppb in 2003 with a simulated global annual mean surface mole fraction of 1577 ppb. This is in good agreement with model simulations conducted by Heimann et al. (2020) using UM-UKCA. The authors report a negative bias of −190 ppb in global annual mean methane surface mole fractions at 1590 ppb. Heimann et al. (2020) argued that the negative bias could be due either to the tropospheric methane sink being too strong in their model or the methane emissions being too low. An identical argument can be made for our model simulations in relation to the negative bias in methane surface mole fractions.

The inlay in Figure 7a shows the evolution of atmospheric methane over the historic period for the whole atmosphere methane burden. The burden shows a very similar trend over the historical period with a maximum negative bias of −600 $Tg(CH_4)$ at an annual mean whole atmosphere methane burden of 4,297 $Tg(CH_4)$ in 2004 of our simulation.

In Figure 7b we examine zonally averaged annual mean methane surface mole fraction anomalies with respect to the global annual mean for three individual latitudinal zones. UKESM1-ems shows an increasing latitudinal divergence in the surface mole fractions from pre-industrial to present-day while there is hardly any north-south gradient present in the concentration-driven simulation over the same period. This is hardly surprising, however, because UKESM1-conc is constrained at the surface with global annual mean values constant over the entire domain (cf. Sellar et al., 2019 and Archibald et al., 2020). The diverging zonally averaged surface mole fraction anomalies in the emission-driven run demonstrate the increasing importance of anthropogenic methane sources over time. Most anthropogenic methane emissions (fossil fuel extraction and use, rice cultivation, cattle raising, landfills) are located north of the equator and even further north in the northern extra-tropics (>23.5°N). Thus, zonally averaged annual mean methane surface mole fraction anomalies are positive (i.e., higher than the global annual mean) only in the northern extratropics between 23.5°N and 90°N. In the tropics and southern extratropics these anomalies become increasingly negative.

The time series of zonally averaged annual mean surface mole fraction anomalies exhibits two maxima in the northern extratropical zone, in 1980 and 2012, respectively. From 1980 to 1997 the methane anomalies in the northern extratropics decrease by 16.9 $Tg(CH_4)$, only to rise again by the same amount by 2012. The minimum in

Figure 7. Global annual mean CH_4 surface mole fraction, expressed in ppb, and estimated residual methane surface exchange flux time series ranging from the pre-industrial (1850) to the present-day (2014), simulated with UKESM1-ems. The figure shows (a) the time series of ensemble mean global mean CH_4 surface mole fractions for UKESM1-conc (black) and UKESM1-ems (red). The inlay in plot (a) depicts the time series of ensemble mean global annual mean CH_4 atmospheric burdens simulated with UKESM1-conc (black) and UKESM1-ems (red), respectively. The shaded area around the individual curves indicates the ensemble spread for each model configuration, expressed as the one standard deviation ($1-\sigma$) interval. Plot (b) shows the difference of ensemble mean annual mean zonally averaged CH_4 surface mole fraction from the global average, expressed in ppb, for three latitudinal bands: the northern extra-tropics (90°N–30°N; dashed lines), the tropics (30°N–30°S; dash-dotted lines) and the southern extra-tropics (30°S–90°S; dotted lines). Red lines refer to simulations with UKESM1-ems and black lines indicate UKESM1-conc simulations. Plot (c) shows estimates of the pre-industrial to present-day time series of the annual global total (solid red line) and decadal average of the annal global total (dashed red line) net residual methane surface exchange flux, expressed in $Tg(CH_4)\ yr^{-1}$, representing the net (positive or negative) methane emissions that are required to bring methane surface mole fractions in UKESM1-ems into complete agreement with the observations, equivalent to the black line in plot (a). The envelope indicates the $1-\sigma$ interval around the decadal means, calculated from the inter-annual variation in annual global totals for each decade.

1997 in the northern extratropics coincides with a maximum in the anomalies in the tropics and southern extratropics. The decrease and subsequent increase in the zonally averaged annual mean surface fraction anomalies in the northern extratropics points to anthropogenic activity as the driving force behind these changes.

We then calculate the residual methane surface flux that would be required to bring surface mole fractions in UKESM1-ems into complete agreement with the observed mole fractions (Figure 7c). Interpreting this residual flux as a "missing source" of methane, this would indicate that a further 50 ± 20 Tg(CH_4) yr^{-1}, on a decadal mean basis at the present day (2000s), would be required for the model to simulate the true rise in methane surface mole fractions. 50 Tg(CH_4) yr^{-1} amounts to approximately 15% and 25% of present-day anthropogenic and wetland methane emissions in our model, respectively.

This is firmly within the uncertainty limits of current emissions estimates for each of the two sources individually (Saunois et al., 2020), and could potentially explain the discrepancy between model and observations. Indeed, in a recently published paper Hmiel et al. (2020) argue that, based on a re-evaluation of the preindustrial-era $^{14}CH_4$ ice-core records, anthropogenic fossil methane emissions could be underestimated by about 38–58 Tg(CH_4) yr^{-1}, or about 25%–40% of recent estimates. This additional anthropogenic methane source would be enough to reconcile our model simulation with observations.

3.4.2. Site-Level Assessment of Methane Surface Mole Fractions

In Figure 8 we compare methane surface mole fractions from UKESM1-conc and UKEMS1-ems with site-level data from stations in the NOAA GML (Global Monitoring Laboratory) Carbon Cycle Cooperative Global Air Sampling Network. Observations have been averaged over all sites contributing to the latitude bands in which they are located.

The left column in Figure 8 (plots a, d, g, and j) shows the time series of annual mean surface mole fraction anomalies with respect to the 2000–2009 mean. In all four latitude bands UKESM1-ems tends to underestimate surface mole fractions between 2000 and 2005. UKESM1-ems also shows an earlier and steeper increase in methane surface mole fractions than the observations starting in 2002–2005 depending on the latitude band. UKESM1-conc follows the observed trend because it is constrained by observations.

We assess the model-to-observations correlation for the annual mean methane surface mole fraction anomalies from UKESM1-conc and UKESM1-ems with those from the observations (shown in the middle column of Figure 8, plots b, e, h, and k) over the period 2000–2009. The plots also include slope and Pearson's correlation coefficient for each of the latitude bands. UKESM1-ems shows a significantly weaker correlation with the observation than UKESM1-conc in all four latitude bands. The weaker correlation is a consequence of the steeper increase in methane surface mole fractions in the second half of the 2000s in UKESM1-ems.

In the right column of Figure 8 (plots c, f, I, and l) we compare multi-annual average monthly mean methane surface mole fraction anomalies (with respect to the annual means) for the period 2000–2009. The observations have been averaged over all sites contributing to each latitude band. UKESM1-conc clearly lacks any seasonal variation in surface methane in all four latitude bands. UKESM1-ems, on the other hand, shows good agreement with the observations with respect to seasonal variation. At northern mid-to high latitudes seasonality in surface methane is over pronounced compared to the observations (Figure 8c) but this overestimation of the seasonal amplitude becomes less pronounced with decreasing latitude (Figures 8f, 8i, and 8l). At southern mid-to high latitudes the picture is reversed with the seasonal variation being more pronounced in the observations than in UKESM1-ems. The comparison of the seasonal variation also reveals a timing error in UKESM1-ems with respect to seasonal maximum and minimum surface methane, which appear approximately one to two months later in the model than in the observations. An interesting exception occurs in the southern mid-to high latitudes, where timing error seems to disappear.

Figure 9 shows the latitudinal distribution of methane in both UKESM1-conc and UKESM1-ems together with latitudinally resolved measurements of methane surface mole fractions from the NOAA GML Air Sampling Network (Dlugokencky et al., 2021). UKESM1-ems yields a maximum interhemispheric gradient of 106 ppb (calculated as the difference between maximum and minimum decadal mean zonally averaged methane surface mole fraction for the period 2000–2009) with a decadal average global mean methane surface mole fraction of 1592 ppb. Heimann et al. (2020) previously reported a methane interhemispheric gradient of 104 ppb with a global mean methane surface mole fraction of 1590 ppb for the period 2000–2005, calculated from their BASE

experiment, which is comparable to our emission-driven simulation (cf. Heimann et al., 2020, Section 3.2). In comparison, the maximum interhemispheric gradient in the observations is approximately 209 ppb with a decadal global mean methane surface mole fraction of 1805 ppb, using the same definition as above.

Driving UKESM1-ems with methane emissions instead of constraining the model at the surface with one value for the methane surface mole fraction that is constant for the entire domain and the whole year, albeit based on observations, represents an obvious improvement in the model's skill in simulating the global methane

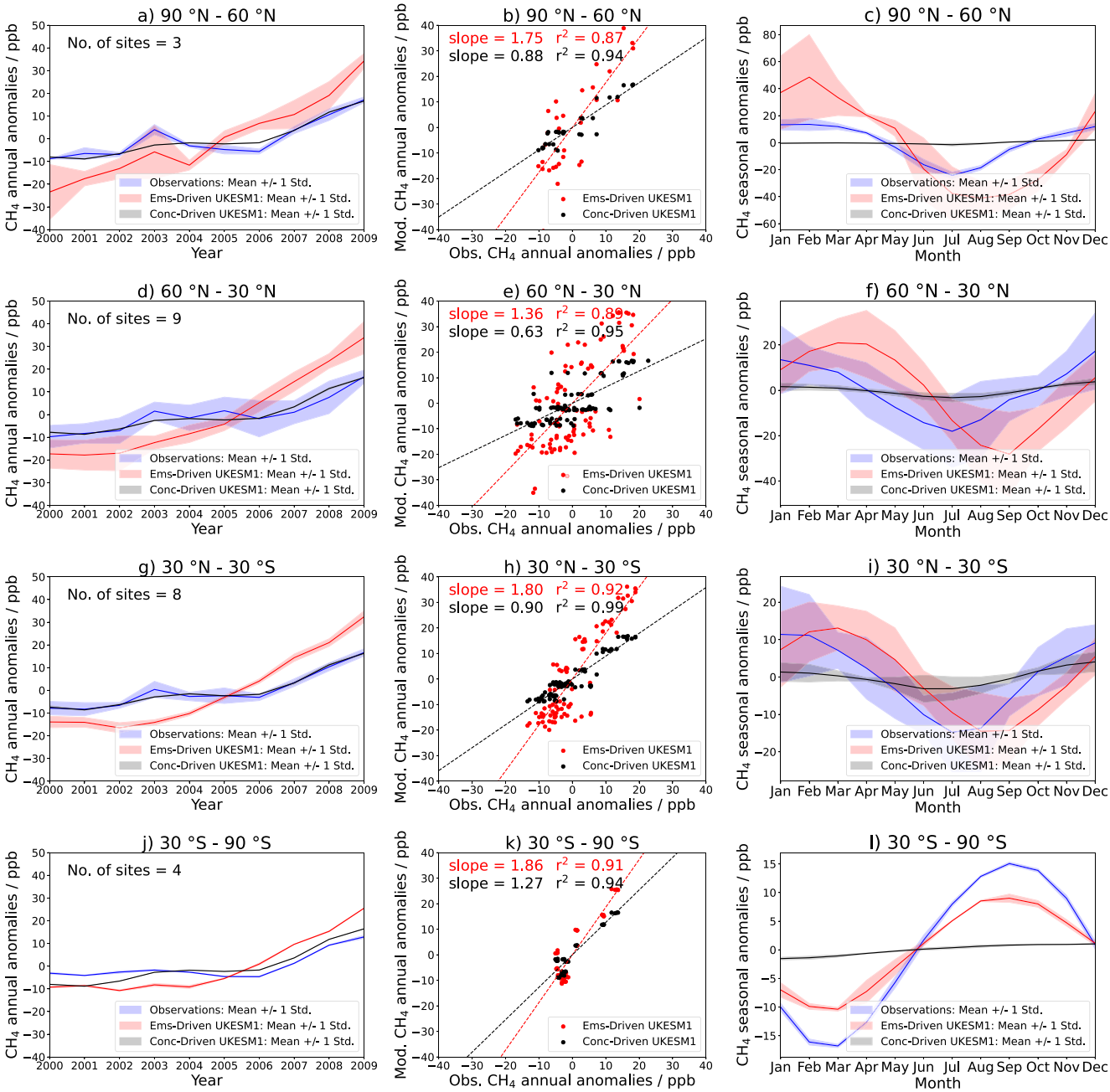

Figure 8. Site-level comparison of the modeled horizontal distribution of methane surface mole fractions from UKESM1-ems with observations from the NOAA GML (Global Monitoring Laboratory) Carbon Cycle Cooperative Global Air Sampling Network. Left column: time series of annual mean methane surface mole fraction anomalies relative to the 2000–2009 mean surface mole fraction at each station for four individual latitude bands. Middle column: UKESM1-ems versus obs correlation for the same four latitude bands. Right column: multi-annual mean seasonal variation in the simulations with UKESM1-ems and observations for the same four latitude bands. Observations are taken from the NOAA GML (Global Monitoring Laboratory) Carbon Cycle Cooperative Global Air Sampling Network, specifically monthly mean flask CH_4 data for the years 2000–2009 (Dlugokencky et al., 2021). UKESM1-ems is represented by one single realisation in each case.

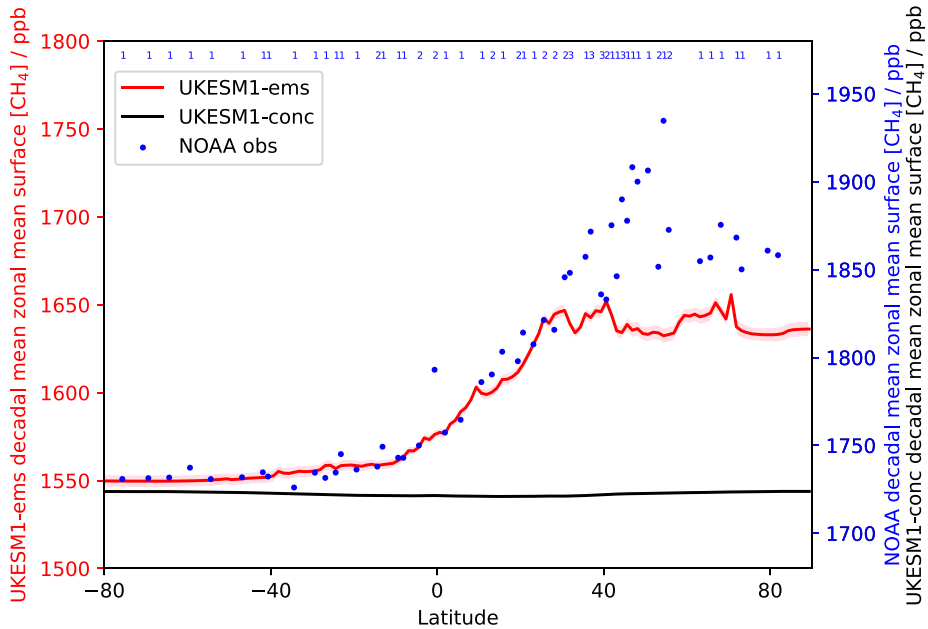

Figure 9. Comparison of methane interhemispheric gradients between UKESM1-ems (red) and UKESM1-conc (black) and observations from the NOAA GML (Global Monitoring Laboratory) Carbon Cycle Cooperative Global Air Sampling Network (Dlugokencky et al., 2021). Methane surface mole fractions in each case have been averaged over the period 2000–2009. Note that the *y*-axes have different values to allow comparison of the interhemispheric gradient (due to the negative bias in UKESM1-ems), but both extend over the same range of 300 ppb.

distribution. This can be seen in Figure 9 and also in Figure 10 which, similar to Figure 6 for modeled carbon monoxide mole fractions, shows the time series differences of the normalized interhemispheric gradients between model and observations.

UKESM1-ems (left plot in Figure 10) shows a substantially better agreement with the methane observation from the NOAA GML station network (Dlugokencky et al., 2021). The only sizable differences in the anomalies are found between 45°N and 55°N after 1993, corresponding to a peak in observed methane surface mole fractions which the model does not capture. In contrast, UKESM1-conc shows substantial negative biases relative to the observations for the entire northern hemisphere over the whole period for which observations are available.

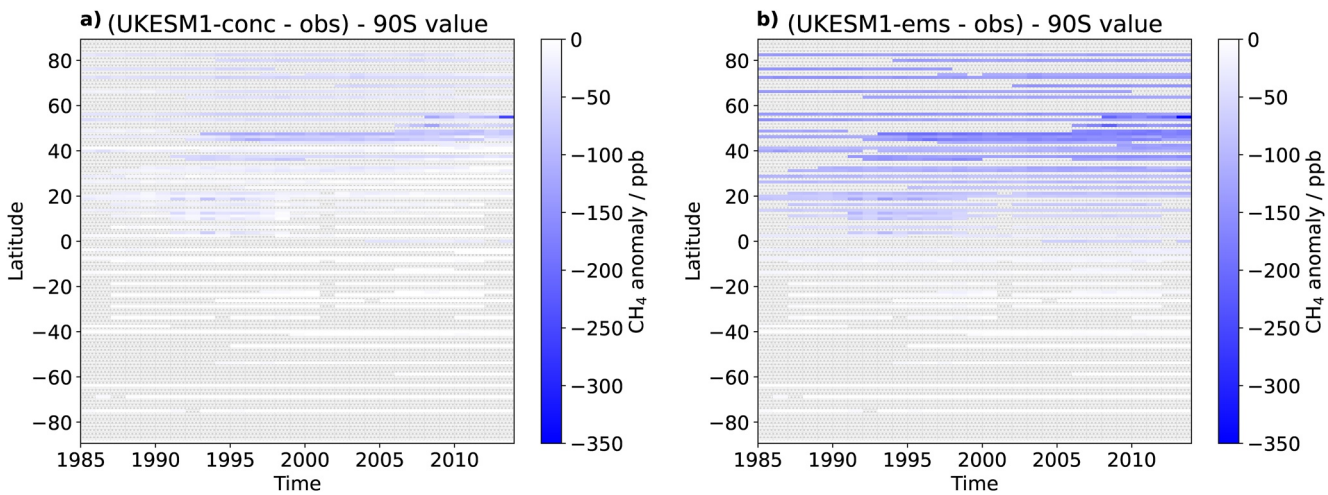

Figure 10. Difference in the time series of the annual zonal mean CH_4 surface mole fraction anomalies (with respect to the CH_4 surface mole fraction at 90°S) for the period 1985–2014 between the simulations and NOAA GML observations (Dlugokencky et al., 2021) for UKESM1-conc (left plot) and UKESM1-ems (right plot). Gray stippling indicates data points for which no observations are available.

3.4.3. Vertical Distribution of Methane

The vertical distribution of methane mole fractions stays relatively constant with increasing height throughout the troposphere because of the relatively long methane chemical lifetime of approximately 9.5 years. Above the tropopause level methane mole fractions begin to drop off. Both configurations of UKESM1 capture this behavior of the methane vertical profile qualitatively. In Figure 11 we compare simulated vertical profiles of normalized zonal mean methane mole fractions with methane observation data from the NASA Atmospheric Tomography Mission (ATom; Wofsy et al., 2021).

In the southern extratropical region (90°–30°S) both model configurations capture the methane vertical profile well up to an altitude of about 7 km. Above 7 km the modeled profiles increasingly diverge from the observed methane profiles; both configurations of UKESM1 show a very similar profile for methane in this latitudinal region. In the tropics methane mole fractions remain virtually constant with height up to the maximum flight altitude of the NASA DC-8 aircraft at approximately 12 km. This is due to a much higher tropopause height in the tropics compared to the extratropical regions. In this latitudinal region the difference between modeled and observed methane profiles is bigger than in the southern extratropics. The methane vertical profiles from UKESM1-ems show a better agreement with observations than those from UKESM1-conc, but the agreement is not as good as in the southern extratropics.

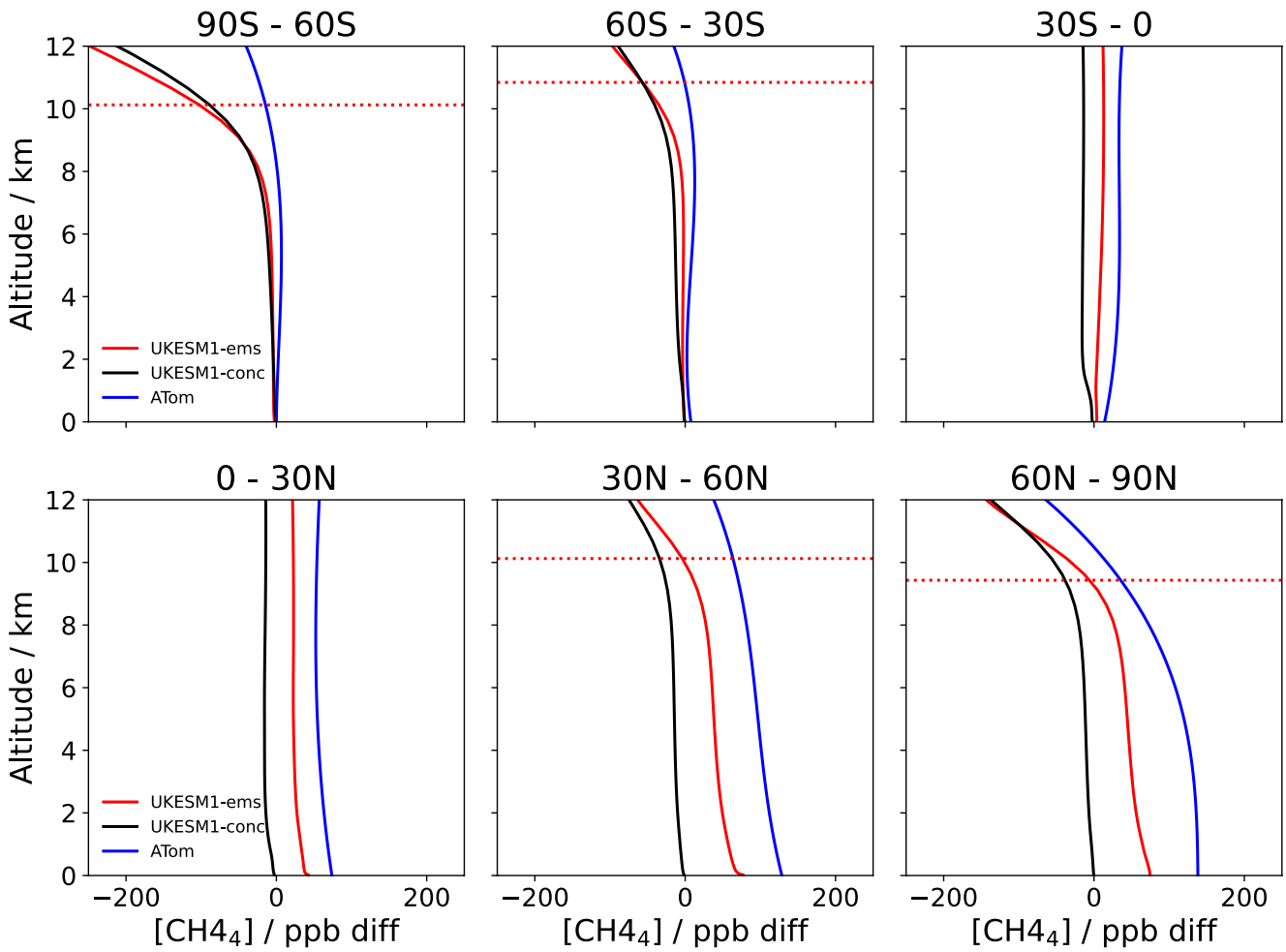

Figure 11. Comparison of vertical profiles of normalized zonal mean CH_4 mole fractions for UKESM1-conc (black) and UKESM1-ems (red) for the year 2000 with methane observations from the Atom (the NASA Atmospheric Tomography Mission; Wofsy et al., 2021) data set (blue). Methane mole fractions in all latitude bands are normalized to the 90°S–60°S mean value. The height of the chemical tropopause (defined as the ozone 150 ppb iso-line) in UKESM1-conc is shown by the red dotted line. ATom profiles extend from 0.2 to 12 km altitude, and flights occurred in each of the four seasons over a 4-year period (2016–2020).

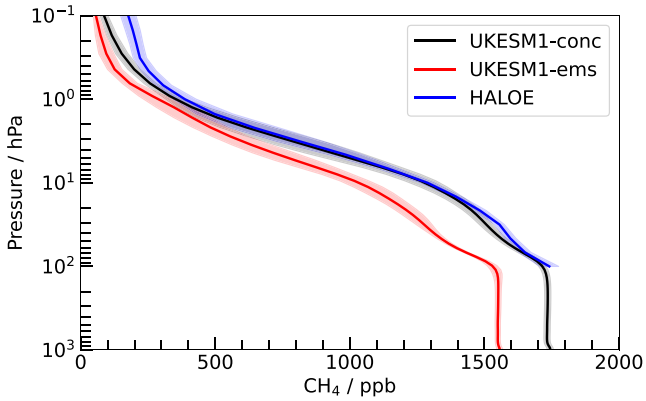

Figure 12. Comparison of multi-year average vertical profiles of the mean tropical (10°N) modeled atmospheric methane mole fraction for the period 1991 to 1997, from UKESM1-conc in black and UKESM1-ems in red with the methane climatology (Kumer et al., 1993) from the Halogen Occultation Experiment (HALOE; Russell et al., 1993) with Cryogenic Limb Array Etalon Spectrometer (CLAES; Roche et al., 1993) instrument on board the NASA Upper Atmosphere Research Satellite (UARS; Reber et al., 1993) in blue over the same period (after Archibald et al., 2020). The shading for each profile represents one standard deviation about the multi-annual mean, except for the HALOE data, where the shading represents the seasonal variation as well as the variation within the tropics.

In the northern extratropical region, our model shows the highest bias relative to the observed methane vertical profile. Also, the difference between the two configurations of UKESM1 is the most pronounced for all latitudinal zones. UKESM1-ems shows a much better agreement with the observed profile than UKESM1-conc throughout the whole troposphere. Interestingly, the methane vertical profile in UKESM1-ems shows a much faster decline with altitude above the tropopause level throughout the northern extratropics (30°N–90°N). Overall, the tropospheric methane vertical profile in UKESM1-ems is in much better agreement with the observations in almost all latitudinal regions than the profiles from the UKESM-conc indicating a substantial improvement in the model's skill to simulate the vertical distribution of methane in the troposphere. While vertical methane mole fraction profiles are practically constant over the entire troposphere, as depicted in Figure 11, methane mole fractions fall off steeply with increasing altitude in the stratosphere.

In Figure 12 we compare vertical profiles of multi-annual mean atmospheric methane mole fractions from UKESM1-ems against methane profiles from UKESM1-conc Also included in Figure 12 is a methane vertical profile of the Halogen Occultation Experiment/Cryogenic Limb Array Etalon Spectrometer (HALOE/CLAES) satellite observation climatology (Kumer et al., 1993; Russell et al., 1993), spanning 1991–1997 (Randel et al., 1998). UKESM1-ems (solid red line in Figure 12) shows a systematic negative bias throughout the stratospheric column, compared to UKESM1-conc (solid black line in Figure 12) which is consistent with the systematic negative bias in methane surface mole fractions (Figure 7) and the tropospheric methane vertical profiles (Figure 11).

The multi-annual zonal mean stratospheric methane distribution is compared against the HALOE/CLAES climatology (Kumer et al., 1993; Russell et al., 1993) in Figure 13. UKESM1-ems shows similar skill in simulating the horizontal and vertical structure of methane in the stratosphere as UKESM1-conc discussed in Archibald et al. (2020). The seasonal variation of stratospheric methane is also well captured (cf. Panels (a) and (b) in Figure 13). UKESM1-ems also shows a negative bias in the absolute methane mole fractions, consistent with the negative bias in tropospheric methane at present-day.

The systematic negative bias in the modeled methane mole fractions is evident for both seasons in the scatter plots (panels (c) and (d) in Figure 13). Root mean square errors have become slightly higher in this configuration at 0.17 ppm as opposed to 0.1 ppm in UKESM1-conc. Slopes are also further away from unity at 0.15, but the correlation between model and observations at $r \geq 0.98$ is equally high as in UKESM1-conc (cf. Archibald et al., 2020; Figure 11). Furthermore, UKESM1-ems simulates equally well the vertical fall-off in methane. There is an excellent one-to-one correspondence between the model and observations: the slopes of the least squares fit for January and July are within 0.05 of unity, the correlation coefficients are greater than 0.98, and the root mean square errors between UKESM1-ems and the HALOE/CLAES climatology are less than 0.1 ppm.

In Figure 14 we compare the total column CH_4 (denoted as XCH_4) calculated from output from UKESM1-ems against satellite observations of XCH_4 (Parker et al., 2020) from the GOSAT satellite (Kuze et al., 2009). The satellite data was first averaged into monthly means with $2° \times 2°$ grid boxes resolution and then the latitudinal mean for each month was computed. For the model data, the total column CH_4 was computed from the vertically resolved model profiles at the native model resolution, with the latitudinal mean then computed from this model-derived XCH_4 data.

Note that the satellite averaging kernels have not been applied to the model output for the following reasons: (a) applying averaging kernels generally requires the model to be sampled at the time and location of the observation, (b) the model's spatial resolution is relatively coarse at $1.9° \times 1.3°$, (c) the GOSAT averaging kernel is relatively flat (Parker et al., 2020) rendering any corrections small in comparison to uncertainties in model and

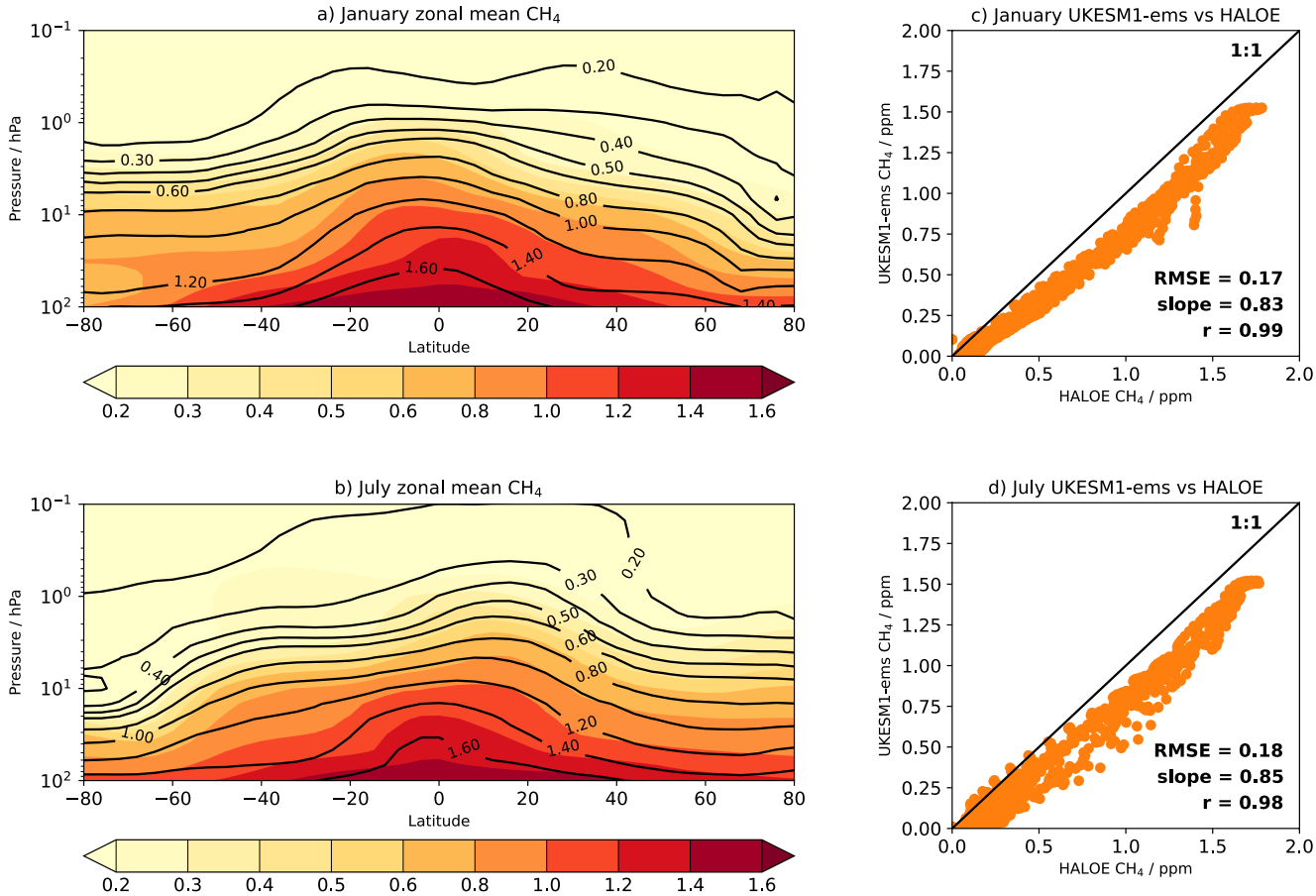

Figure 13. Comparison of multi-annual mean monthly mean zonal mean stratospheric methane mole fractions (expressed in ppm) from the historical UKESM1-ems simulation with the HALOE/CLAES methane climatology (cf., Kumer et al., 1993; HALOE; Russell et al., 1993; CLAES; Roche et al., 1993; UARS; Reber et al., 1993) for the period 1991–1997. The comparison is for zonal mean stratospheric methane mole fractions for January and July in panels (a) and (b) and scatter plots of modeled vs. observed mole fractions for January and July in panels (c) and (d), respectively. The filled color contours in panels (a) and (b) represent data from UKESM1-ems and the black contour lines represent the HALOE/CLAES climatology. The scatter plots also show the 1:1-correlation line, the root mean square errors, the slope of a least squares linear fit, and the Pearson correlation coefficient (r).

observations, and (d) the averaging kernel is constant over time and omitting it will not introduce errors in seasonality and interannual variability. For these reasons the potential correction was deemed to be insignificant compared to the existing systematic negative bias between the model and observations.

The zonal and temporal distribution of total column methane in UKESM1-ems is in excellent qualitative agreement with the observations. The model shows a similar interhemispheric gradient in XCH_4. Both data sets show a very similar methane trend over the 10 years of the observed period (2010–2020). Model and observations also agree on the amplitude in the seasonality in both hemispheres, with a small timing error discernible in the model simulation: the model seems to lag behind persistently with respect to the observed XCH_4 by one or two months. Overall, the qualitative agreement between modeled and observed XCH_4 is very strong.

As noted in Section 3.4, an offset of approximately 200 ppb was identified between modeled methane surface mole fractions and observations at present-day conditions (2000s). This offset persists in the total column comparisons, with a negative bias in the model of approximately 180 ppb. To facilitate comparison, we have removed the negative bias in Figure 14, simply by adjusting the scales in each of the plots. However, the scales extend over the same range of 190 ppb in each of the two subplots.

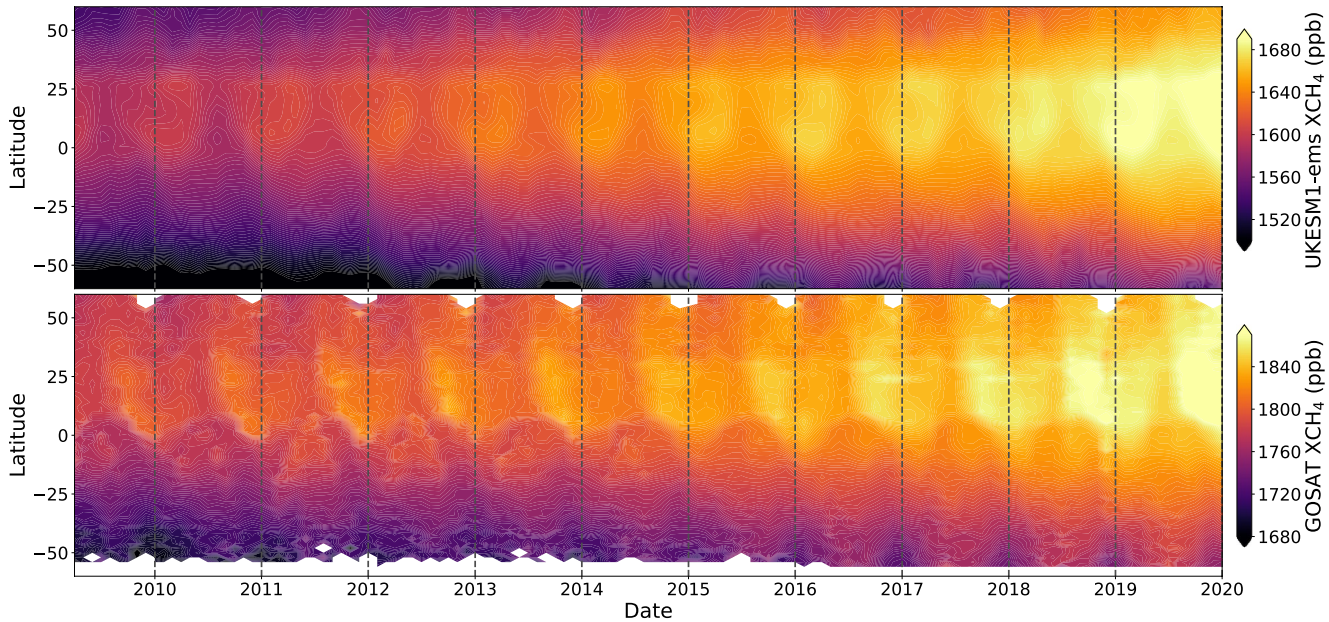

Figure 14. Hovmöller plot (zonal mean vs. time) comparing the total column CH_4 (XCH_4) latitude-time distribution calculated from UKESM1-ems model data and GOSAT satellite (Kuze et al., 2009) XCH_4 data (Parker et al., 2020). Scales in each subplot have been chosen to remove the systematic negative bias in the model data but they extend over the same range of 190 ppb. For this figure, model data beyond 2014 is taken from a future scenario simulation with UKESM1-esm. The future scenario simulation applies the Shared Socio-economic pathway, SSP, scenarios (Gidden et al., 2019), provided for Coupled Model Intercomparison Project–Phase 6, using SSP3-7.0. However, for the first few years SSP scenarios differ very little.

4. Discussion and Conclusions

In this paper we have described a new, methane emission-driven configuration of the first community release version of the UK Earth System Model, UKESM1.0. This new capability for ESMs will enable a fuller and more realistic simulation of the global methane cycle. In the same way in which emissions-driven CO_2 simulations have enabled much more policy-relevant science to be explored with climate models (Arora et al., 2020; Friedlingstein et al., 2006) this interactive capability will enable ESMs to address more directly and consistently forcing and feedbacks associated with methane.

Our focus has been on the assessment of the model's capability to simulate the main methane sources, particularly the fully coupled methane wetland emission model, and sinks and its atmospheric abundance over the historic period 1850–2014. We have presented the areas of improvement over the default, UKESM1-conc (cf., Sellar et al., 2019, 2020; Archibald et al., 2020; Mulcahy et al., 2020) and we have identified the areas for which systematic biases persist in the new configuration.

Our evaluation has shown that UKESM1-ems simulates all the components of the methane cycle within observational uncertainty. We found that the UKESM1-ems simulation of the global annual mean methane surface mole fraction is in excellent agreement with observations for the first half of the historic period from 1850 to approximately the 1920s, a period during which natural methane emission sources dominated. After about 1920 the model shows an increasing negative bias in simulating atmospheric methane mole fractions. During this latter period between the 1920s and present-day anthropogenic methane emission became increasingly important in the global methane budget. It is not possible to say from this initial assessment whether this underestimation of the atmospheric methane burden is a model bias in simulated processes or an underestimate of historical emissions from CMIP6 used to drive the simulations. One recommendation therefore from our study is that better estimates and reconstructions of past CH_4 emissions are needed.

This is analogous to the uncertainty in past CO_2 emissions - which is especially large for emissions from land-use and land-use change, and which hinders the simulation of past CO_2 being used as a constraint on future projections (Booth et al., 2017). In the meantime, process-based and site-specific evaluation against a range of observations

and chemical species gives us confidence that the model is performing well and is fit for purpose for exploration of future changes in the methane cycle.

While studies in the past have dealt with certain aspects of the methane cycle and feedbacks with climate (cf., e.g., Holmes, C. D., 2018; Gedney et al., 2019; Nguyen et al., 2020, Stevenson et al., 2020), these processes have been absent from mainstream climate model projections contributing to past CMIP simulations. This new capability will enable assessment of future emissions and mitigation pathways (Staniaszek et al., 2022) and even the implications and potential benefits of anthropogenic methane removal (Abernethy et al., 2021; Jackson et al., 2021).

Interactions between biogeochemical cycles can also be investigated using this new capability. For example, changes in atmospheric CO_2 may stimulate CH_4 emissions from wetlands (a major uncertainty in future emissions: Canadell et al., 2021), thawing of permafrost may release large amounts of CH_4 as well as CO_2 (Burke et al., 2012) and changes in wildfire activity not only represent potential abrupt changes to ecosystems but could increase CH_4 and aerosol emissions. These new feedbacks have the potential to alter the global climate sensitivity–usually defined as the climate response to elevated CO_2, but in a fully coupled system may also include the subsequent changes in atmospheric composition.

It is worthwhile noting here that UKESM1-ems is capable of correctly simulating the recent changes in the atmospheric methane trends (cf. Figure 7a). The model reproduces the hiatus in the methane growth between approximately 1999 and 2006 (Allen, 2016) and the renewed rise in atmospheric methane trends after this period (Schaefer, 2019). Hence, the new capability in simulating the global methane cycle fully interactively will allow us to examine possible mechanisms behind the recent hiatus in substantially more detail than was possible hitherto. We will address this question in a follow-up study.

In this paper we have made no attempt to explain in detail the causes for the model biases identified here because it is beyond this initial model assessment. Further studies are planned which will address the biases with targeted follow-up studies on:

1. The cause(s) behind the systematic negative bias in the methane surface mole fraction and atmospheric burden
2. The assessment of the sensitivities and uncertainties in the wetland emissions in UKESM1-ems and their main drivers: climate change versus CO_2 fertilisation effects.
3. The assessment of the climate sensitivity in UKESM1-ems
4. The assessment of the timing errors in the seasonality of the atmospheric methane burden
5. The assessment of the biases in CO surface mole fractions in UKESM1-ems

We want to conclude this discussion with a broader perspective on the performance of UKESM1-ems for the purpose of carbon cycle analysis by comparing it with the three development cycles of CO_2 emission-driven coupled carbon cycle models over the past 20 years. We look at the relative error in simulating the pre-industrial-to-present-day increase in atmospheric CO_2 over four generations of emission-driven coupled carbon cycle models with the relative error in simulating the increase in atmospheric methane in UKESM1-ems (cf. Figure 15). UKESM1-ems is representative of the first generation of a new, substantially more complex type of carbon cycle models that also includes an interactive coupling to atmospheric composition.

Figure 15 clearly shows the significant improvement in the performance of every generation of emission-driven coupled carbon cycle models with substantially reduced relative errors in simulating the PI-to-PD increase in CO_2. While the first generation of these models showed a 40% relative error this has been reduced to a mere 10% in the latest generation of coupled carbon cycle models. For the first version of UKESM1-ems we find a 20% relative error in simulating the PI-to-PD increase in atmospheric methane mole fractions which is comparable to the performance of the majority of coupled carbon cycle models participating in CMIP5 in simulating the PI-to-PD CO_2 increase. It is our hope that UKESM1-ems, while already showing a good performance, will also follow the path of substantial improvements in understanding and representation of the global carbon cycle and its feedbacks with the land surface, atmospheric composition and the climate and Earth systems in its future versions.

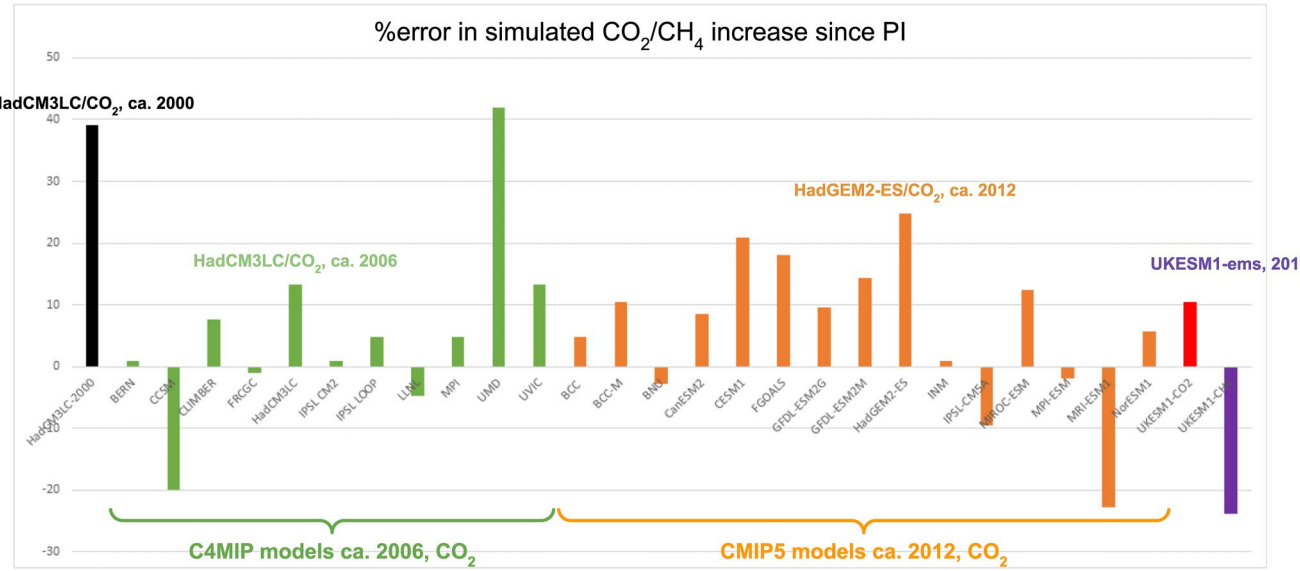

Figure 15. Comparison of the relative error (%) in the simulated CO_2 mole fraction increase since the pre-industrial over the past 20 years of emission-driven carbon cycle modeling. Black: Cox et al. (2000); green: Climate–Carbon Cycle Feedback Analysis from C4MIP (Friedlingstein et al., 2006); orange: Carbon cycle feedbacks in Coupled Model Intercomparison Project–Phase 5 (CMIP5) simulations (Friedlingstein et al., 2014); red: CMIP6 CO_2 simulation with the UKESM1 standard configuration; purple: UKESM1-ems simulation, but for methane (this work).

Acknowledgments
This work was supported by the Joint UK BEIS/Defra Met Office Hadley Centre Climate Programme (GA01101) and the European Union projects CRESCENDO (under grant agreement No 641816) and ESM2025 (under grant agreement No 101003536). ZS was funded by the NERC C-CLEAR DTP (NE/S007164/1). ATA, PTG were funded through NCAS and acknowledge the NERC ACSIS LTSM for support. UKCA is supported by the Met Office and NCAS through the JWCRP who we thank for support. RJP is funded via the UK National Centre for Earth Observation (NE/N018079/1). This research used the ALICE High Performance Computing Facility at the University of Leicester for the GOSAT retrievals and analysis. We thank the Japanese Aerospace Exploration Agency, National Institute for Environmental Studies, and the Ministry of Environment for the GOSAT data and their continuous support as part of the Joint Research Agreement. We also wish to thank Ed Dlugokencky and colleagues from NOOA/GML for providing observational methane data sets from the GML global station network used in the preparation of CH_4 surface mole fraction anomalies. We are grateful to Zhen Zhang and Ben Poulter for helping us with the WADM2v2 data set and Steven Wofsy and the ATom team for providing the ATom aircraft data set. The authors also wish to thank the editor and three anonymous referes for their valuable comments and suggestions that helped improve the manuscript considerably.

Data Availability Statement

Model and observation data sets used in this manuscript are publicly available via Zenodo (https://doi.org/10.5281/zenodo.6553281) under the Open Government Licence. In addition, methane atmospheric mole fraction data from the NOAA/GML station network can be obtained from their website (https://gml.noaa.gov/ccgg/trends_ch4/). ATom aircraft data for CH_4 and CO can be obtained from the NASA ESPO ATom website (https://espo.nasa.gov/atom). The WADM2 data set used in preparing this manuscript has been made available here: https://drive.google.com/file/d/1g8AABp_Ny44VyC9VTxak-nmcEL-31EaM/view. All the code that was used to produce the results presented in this manuscript in the table and figures has been made available via the same Zenodo project repository (https://doi.org/10.5281/zenodo.6553281) as was used for the data sets.

References

Abernethy, S., O'Connor, F. M., Jones, C. D., & Jackson, R. B. (2021). Methane removal and the proportional reductions in surface temperature and ozone. *Philosophical Transactions of the Royal Society A*, *379*(2210), 20210104. https://doi.org/10.1098/rsta.2021.0104

Allen, G. (2016). Rebalancing the global methane budget. *Nature*, *538*(7623), 46–48. https://doi.org/10.1038/538046a

Archibald, A. T., O'Connor, F. M., Abraham, N. L., Archer-Nicholls, S., Chipperfield, M. P., Dalvi, M., et al. (2020). Description and evaluation of the UKCA stratosphere–troposphere chemistry scheme (StratTrop vn 1.0) implemented in UKESM1. *Geoscientific Model Development*, *13*(3), 1223–1266. https://doi.org/10.5194/gmd-13-1223-2020

Arora, V. K., Katavouta, A., Williams, R. G., Jones, C. D., Brovkin, V., Friedlingstein, P., et al. (2020). Carbon–concentration and carbon–climate feedbacks in CMIP6 models and their comparison to CMIP5 models. *Biogeosciences*, *17*(16), 4173–4222. https://doi.org/10.5194/bg-17-4173-2020

Bastviken, D., Tranvik, L. J., Downing, J. A., Crill, P. M., & Enrich-Prast, A. (2011). Freshwater methane emissions offset the continental carbon sink. *Science*, *331*(6013), 50. https://doi.org/10.1126/science.1196808

Best, M. J., Pryor, M., Clark, D. B., Rooney, G. G., Essery, R. L. H., Ménard, C. B., et al. (2011). The Joint UK land environment simulator (JULES), model description – Part 1: Energy and water fluxes. *Geoscientific Model Development*, *4*(3), 677–699. https://doi.org/10.5194/gmd-4-677-2011

Booth, B. B. B., Harris, G. R., Murphy, J. M., House, J. I., Jones, C. D., Sexton, D., & Sitch, S. (2017). Narrowing the range of future climate projections using historical observations of atmospheric CO_2. *Journal of Climate*, *30*(8), 3039–3053. https://doi.org/10.1175/jcli-d-16-0178.1

Burke, E. J., Chadburn, S. E., & Ekici, A. (2017). A vertical representation of soil carbon in the JULES land surface scheme (vn4.3_permafrost) with a focus on permafrost regions. *Geoscientific Model Development*, *10*(2), 959–975. https://doi.org/10.5194/gmd-10-959-2017

Burke, E. J., Hartley, I. P., & Jones, C. D. (2012). Uncertainties in the global temperature change caused by carbon release from permafrost thawing. *The Cryosphere*, *6*, 1063–1076. https://doi.org/10.5194/tc-6-1063-2012

Canadell, J. G., Monteiro, P. M. S., Costa, M. H., Da Cunha, L. C., Lebehot, A. D., Cox, P. M., et al. (2021). Global carbon and other biogeochemical cycles and feedbacks. *IPCC AR6 WGI, Final Government Distribution, chapter 5*. hal-03336145.

Clark, D. B., Mercado, L. M., Sitch, S., Jones, C. D., Gedney, N., Best, M. J., et al. (2011). The Joint UK Land Environment Simulator (JULES), model description part 2: Carbon fluxes and vegetation dynamics. *Geoscientific Model Development*, *4*(3), 701–722. https://doi.org/10.5194/gmd-4-701-2011

Collins, W. J., Bellouin, N., Doutriaux-Boucher, M., Gedney, N., Halloran, P., Hinton, T., et al. (2011). Development and evaluation of an Earth-System model – HadGEM2. *Geoscientific Model Development*, *4*, 1051–1075. https://doi.org/10.5194/gmd-4-1051-2011

Collins, W. J., Lamarque, J.-F., Schulz, M., Boucher, O., Eyring, V., Hegglin, M. I., et al. (2017). AerChemMIP: Quantifying the effects of chemistry and aerosols in CMIP6. *Geoscientific Model Development*, *10*(2), 585–607. https://doi.org/10.5194/gmd-10-585-2017

Cox, P., Betts, R., Jones, C., Spall, S. A., & Totterdell, I. J. (2000). Acceleration of global warming due to carbon-cycle feedbacks in a coupled climate model. *Nature*, *408*(6809), 184–187. https://doi.org/10.1038/35041539

Dlugokencky, E., & Tans, P. (2020). NOAA/GML. https://gml.noaa.gov/ccgg/trends/gl_data.html

Dlugokencky, E. J., Crotwell, A. M., Mund, J. W., Crotwell, M. J., & Thoning, K. W. (2021). Atmospheric methane dry air mole fractions from the NOAA GML carbon cycle cooperative global air sampling network, 1983-2020, version: 2021-07-30, https://doi.org/10.15138/VNCZ-M766

Eyring, V., Bony, S., Meehl, G. A., Senior, C. A., Stevens, B., Stouffer, R. J., & Taylor, K. E. (2016). Overview of the coupled model Intercomparison project Phase 6 (CMIP6) experimental design and organization. *Geoscientific Model Development*, *9*(5), 1937–1958. https://doi.org/10.5194/gmd-9-1937-2016

Fiore, A. M., Dentener, F. J., Wild, O., Cuvelier, C., Schultz, M. G., Hess, P., et al. (2009). Multimodel estimates of intercontinental source-receptor relationships for ozone pollution. *Journal of Geophysical Research*, *114*(D4), D04301. https://doi.org/10.1029/2008JD010816

Forster, P., Storelvmo, T., Armour, K., Collins, W., Dufresne, J. L., Frame, D., et al. (2021). The Earth's energy budget, climate feedbacks, and 39 climate sensitivity. In V. Masson-Delmotte, P. Zhai, A. Pirani, S. L. Connors, S. Berger, N. Caud, et al. (Eds.), *Climate change 2021: The physical science basis. Contribution of working group I 40 to the sixth assessment report of the intergovernmental panel on climate change*. Cambridge University Press.

Friedlingstein, P., Cox, P., Betts, R., Bopp, L., Brovkin, V., Cadule, P., et al. (2006). Climate–carbon cycle feedback analysis: Results from the C4MIP model Intercomparison. *Journal of Climate*, *19*(14), 3337–3353. https://doi.org/10.1175/jcli3800.1

Friedlingstein, P., Meinshausen, M., Arora, V. K., Jones, C. D., Anav, A., Liddicoat, S. K., & Knutti, R. (2014). Uncertainties in CMIP5 climate projections due to carbon cycle feedbacks. *Journal of Climate*, *27*(2), 511–526. https://doi.org/10.1175/jcli-d-12-00579.1

Fung, I., John, J., Lerner, J., Matthews, E., Prather, M., Steele, L. P., & Fraser, P. J. (1991). Three-dimensional model synthesis of the global methane cycle. *Journal of Geophysical Research*, *96*(D7), 13033–13065. https://doi.org/10.1029/91JD01247

Ganesan, A. L., Schwietzke, S., Poulter, B., Arnold, T., Lan, X., Rigby, M., et al. (2019). Advancing scientific understanding of the global methane budget in support of the Paris Agreement. *Global Biogeochemical Cycles*, *33*(12), 1475–1512. https://doi.org/10.1029/2018GB006065

Gedney, N., & Cox, P. M. (2003). The sensitivity of global climate model simulations to the representation of soil moisture heterogeneity. *Hydrometallurgy*, *4*(6), 1265–1275. https://doi.org/10.1175/1525-7541(2003)004<1265:tsogcm>2.0.co;2

Gedney, N., Cox, P. M., & Huntingford, C. (2004). Climate feedback from wetland methane emissions. *Geophysical Research Letters*, *31*(20), L20503. https://doi.org/10.1029/2004GL020919

Gedney, N., Huntingford, C., Comyn-Platt, E., & Wiltshire, A. (2019). Significant feedbacks of wetland methane release on climate change and the causes of their uncertainty. *Environmental Research Letters*, *14*(8), 084027. https://doi.org/10.1088/1748-9326/ab2726

Gidden, M. J., Riahi, K., Smith, S. J., Fujimori, S., Luderer, G., Kriegler, E., et al. (2019). Global emissions pathways under different socioeconomic scenarios for use in CMIP6: A data set of harmonized emissions trajectories through the end of the century. *Geoscientific Model Development*, *12*(4), 1443–1475. https://doi.org/10.5194/gmd-12-1443-2019

Granier, C., Guenther, A., Lamarque, J. F., Mieville, A., Muller, J. F., Olivier, J., et al. (2005). POET, a database of surface emissions of ozone precursors, available on the internet at. Retrieved from http://www.aero.jussieu.fr/projet/ACCENT/POET.php

Griffiths, P. T., Murray, L. T., Zeng, G., Shin, Y. M., Abraham, N. L., Archibald, A. T., et al. (2021). Tropospheric ozone in CMIP6 simulations. *Atmospheric Chemistry and Physics*, *21*(5), 4187–4218. https://doi.org/10.5194/acp-21-4187-2021

Haney, R. L. (1971). Surface thermal boundary condition for ocean circulation models. *Journal of Physical Oceanography*, *1*(4), 241–248. https://doi.org/10.1175/1520-0485(1971)001<0241:stbcfo>2.0.co;2

Harper, A. B., Cox, P. M., Friedlingstein, P., Wiltshire, A. J., Jones, C. D., Sitch, S., et al. (2016). Improved representation of plant functional types and physiology in the Joint UK Land Environment Simulator (JULES v4.2) using plant trait information. *Geoscientific Model Development*, *9*(7), 2415–2440. https://doi.org/10.5194/gmd-9-2415-2016

Harper, A. B., Wiltshire, A. J., Cox, P. M., Friedlingstein, P., Jones, C. D., Mercado, L. M., et al. (2018). Vegetation distribution and terrestrial carbon cycle in a carbon cycle configuration of JULES4.6 with new plant functional types. *Geoscientific Model Development*, *11*(7), 2857–2873. https://doi.org/10.5194/gmd-11-2857-2018

Heimann, I., Griffiths, P. T., Warwick, N. J., Abraham, N. L., Archibald, A. T., & Pyle, J. A. (2020). Methane emissions in a chemistry-climate model: Feedbacks and climate response. *Journal of Advances in Modeling Earth Systems*, *12*(10), e2019MS002019. https://doi.org/10.1029/2019MS002019

Hmiel, B., Petrenko, V. V., Dyonisius, M. N., Buizert, C., Smith, A. M., Place, P. F., et al. (2020). Preindustrial $^{14}CH_4$ indicates greater anthropogenic fossil CH_4 emissions. *Nature*, *578*(7795), 409–412. https://doi.org/10.1038/s41586-020-1991-8

Hoesly, R. M., Smith, S. J., Feng, L., Klimont, Z., Janssens-Maenhout, G., Pitkanen, T., et al. (2018). Historical (1750–2014) anthropogenic emissions of reactive gases and aerosols from the community emissions data system (CEDS). *Geoscientific Model Development*, *11*(1), 369–408. https://doi.org/10.5194/gmd-11-369-2018

Holmes, C. D. (2018). Methane feedback on atmospheric chemistry: Methods, models, and mechanisms. *Journal of Advances in Modeling Earth Systems*, *10*(4), 1087–1099. https://doi.org/10.1002/2017MS001196

Hopcroft, P., Valdes, P., O'Connor, F., Kaplan, J. O., & Beerling, D. J. (2017). Understanding the glacial methane cycle. *Nature Communications*, *8*(1), 14383. https://doi.org/10.1038/ncomms14383

Jackson, R. B., Sam, A., Canadell Josep, G., Matteo, C., Davis Steven, J., Féron, S., et al. (2021). Atmospheric methane removal: A research agenda. *Philosophical Transactions of the Royal Society A*, *379*(2210), 20200454. https://doi.org/10.1098/rsta.2020.0454

Jones, C. D., Hughes, J. K., Bellouin, N., Hardiman, S. C., Jones, G. S., Knight, J., et al. (2011). The HadGEM2-ES implementation of CMIP5 centennial simulations. *Geoscientific Model Development*, *4*(3), 543–570. https://doi.org/10.5194/gmd-4-543-2011

Kirschke, S., Bousquet, P., Ciais, P., Saunois, M., Canadell, J. G., Dlugokencky, E. J., et al. (2013). Three decades of global methane sources and sinks. *Nature Geoscience*, *6*(10), 813–823. https://doi.org/10.1038/ngeo1955

Kuhlbrodt, T., Jones, C. G., Sellar, A., Storkey, D., Blockley, E., Stringer, M., et al. (2018). The low–resolution version of HadGEM3 GC3.1: Development and evaluation for global climate. *Journal of Advances in Modeling Earth Systems*, *10*(11), 2865–2888. https://doi.org/10.1029/2018MS001370

Kumer, J. B., Mergenthaler, J. L., & Roche, A. E. (1993). CLAES CH_4, N_2O and CCl_2F_2 (F12) global data. *Geophysical Research Letters*, *20*(12), 1239–1242. https://doi.org/10.1029/93gl01341

Kuze, A., Suto, H., Nakajima, M., & Hamazaki, T. (2009). Thermal and near infrared sensor for carbon observation Fourier-transform spectrometer on the Greenhouse Gases Observing Satellite for greenhouse gases monitoring. *Applied Optics*, *48*(35), 6716–6733. https://doi.org/10.1364/AO.48.006716

Lamarque, J.-F., Bond, T. C., Eyring, V., Granier, C., Heil, A., Klimont, Z., et al. (2010). Historical (1850–2000) gridded anthropogenic and biomass burning emissions of reactive gases and aerosols: Methodology and application. *Atmospheric Chemistry and Physics*, *10*(15), 7017–7039. https://doi.org/10.5194/acp-10-7017-2010

Lamarque, J.-F., Shindell, D. T., Josse, B., Young, P. J., Cionni, I., Eyring, V., et al. (2013). The atmospheric chemistry and climate model Intercomparison project (ACCMIP): Overview and description of models, simulations and climate diagnostics. *Geoscientific Model Development*, *6*(1), 179–206. https://doi.org/10.5194/gmd-6-179-2013

Lawrence, M. G., Jöckel, P., & von Kuhlmann, R. (2001). What does the global mean OH concentration tell us? *Atmospheric Chemistry and Physics*, *1*, 37–49. https://doi.org/10.5194/acp-1-37-2001

Lelieveld, J., Gromov, S., Pozzer, A., & Taraborrelli, D. (2016). Global tropospheric hydroxyl distribution, budget and reactivity. *Atmospheric Chemistry and Physics*, *16*(19), 12477–12493. https://doi.org/10.5194/acp-16-12477-2016

Mangeon, S., Voulgarakis, A., Gilham, R., Harper, A., Sitch, S., & Folberth, G. (2016). Inferno: A fire and emissions scheme for the UK Met office's unified model. *Geoscientific Model Development*, *9*(8), 2685–2700. https://doi.org/10.5194/gmd-9-2685-2016

Mao, J., Fan, S., Jacob, D. J., & Travis, K. R. (2013). Radical loss in the atmosphere from Cu-Fe redox coupling in aerosols. *Atmospheric Chemistry and Physics*, *13*(2), 509–519. https://doi.org/10.5194/acp-13-509-2013

McNorton, J., Gloor, E., Wilson, C., Hayman, G. D., Gedney, N., Comyn-Platt, E., et al. (2016). Role of regional wetland emissions in atmospheric methane variability. *Geophysical Research Letters*, *43*(21), 11433–11444. https://doi.org/10.1002/2016GL070649

Meinshausen, M., Vogel, E., Nauels, A., Lorbacher, K., Meinshausen, N., Etheridge, D. M., et al. (2017). Historical greenhouse gas concentrations for climate modelling (CMIP6). *Geoscientific Model Development*, *10*, 2057–2116. https://doi.org/10.5194/gmd-10-2057-2017

Mulcahy, J. P., Johnson, C., Jones, C. G., Povey, A. C., Scott, C. E., Sellar, A., et al. (2020). Description and evaluation of aerosol in UKESM1 and HadGEM3-GC3.1 CMIP6 historical simulations. *Geoscientific Model Development*, *13*(12), 6383–6423. https://doi.org/10.5194/gmd-13-6383-2020

Naik, V., Voulgarakis, A., Fiore, A. M., Horowitz, L. W., Lamarque, J.-F., Lin, M., et al. (2013). Preindustrial to present-day changes in tropospheric hydroxyl radical and methane lifetime from the Atmospheric Chemistry and Climate Model Intercomparison Project (ACCMIP). *Atmospheric Chemistry and Physics*, *13*(10), 5277–5298. https://doi.org/10.5194/acp-13-5277-2013

Nazarenko, L. S., Tausnev, N., Russell, G. L., Rind, D., Miller, R. L., Schmidt, G. A., et al. (2022). Future climate change under SSP emission scenarios with GISS-E2.1. *Journal of Advances in Modeling Earth Systems*, *14*, e2021MS002871. https://doi.org/10.1029/2021MS002871

Nguyen, N. H., Turner, A. J., Yin, Y., Prather, M. J., & Frankenberg, C. (2020). Effects of chemical feedbacks on decadal methane emissions estimates. *Geophysical Research Letters*, *47*(3), e2019GL085706. https://doi.org/10.1029/2019GL085706

Nicely, J. M., Canty, T. P., Manyin, M., Oman, L. D., Salawitch, R. J., Steenrod, S. D., et al. (2018). Changes in global tropospheric OH expected as a result of climate change over the last several decades. *Journal of Geophysical Research: Atmospheres*, *123*(18), 10774–10795. https://doi.org/10.1029/2018JD028388

O'Connor, F. M., Johnson, C. E., Morgenstern, O., Abraham, N. L., Braesicke, P., Dalvi, M., et al. (2014). Evaluation of the new UKCA climate-composition model – Part 2: The Troposphere. *Geoscientific Model Development*, *7*, 41–91. https://doi.org/10.5194/gmd-7-41-2014

O'Neill, B. C., Tebaldi, C., van Vuuren, D. P., Eyring, V., Friedlingstein, P., Hurtt, G., et al. (2016). The scenario model Intercomparison project (ScenarioMIP) for CMIP6. *Geoscientific Model Development*, *9*, 3461–3482. https://doi.org/10.5194/gmd-9-3461-2016

Parker, R. J., Webb, A., Boesch, H., Somkuti, P., Barrio Guillo, R., Di Noia, A., et al. (2020). A decade of GOSAT Proxy satellite CH4 observations. *Earth System Science Data*, *12*(4), 3383–3412. https://doi.org/10.5194/essd-12-3383-2020

Prather, M. J. (1994). Lifetimes and eigenstates in atmospheric chemistry. *Geophysical Research Letters*, *21*(9), 801–804. https://doi.org/10.1029/94GL00840

Prather, M. J., Holmes, C. D., & Hsu, J. (2012). Reactive greenhouse gas scenarios: Systematic exploration of uncertainties and the role of atmospheric chemistry. *Geophysical Research Letters*, *39*(9), L09803. https://doi.org/10.1029/2012GL051440

Prinn, R. G., Huang, J., Weiss, R. F., Cunnold, D. M., Fraser, P. J., Simmonds, P. G., et al. (2005). Evidence for variability of atmospheric hydroxyl radicals over the past quarter century. *Geophysical Research Letters*, *32*(7), L07809. https://doi.org/10.1029/2004GL022228

Quiquet, A., Archibald, A. T., Friend, A. D., Chappellaz, J., Levine, J. G., Stone, E. J., et al. (2015). The relative importance of methane sources and sinks over the Last Interglacial period and into the last glaciation. *Quaternary Science Reviews*, *112*, 1–16. https://doi.org/10.1016/j.quascirev.2015.01.004

Randel, W. J., Wu, F., Russell, J. M., III, Roche, A., & Waters, J. W. (1998). Seasonal cycles and QBO variations in stratospheric CH_4 and H_2O observed in UARS HALOE data. *Journal of the Atmospheric Sciences*, *55*(2), 163–185. https://doi.org/10.1175/1520-0469(1998)055<0163:scaqvi>2.0.co;2

Reber, C. A., Trevathan, C. E., McNeal, R. J., & Luther, M. R. (1993). The upper atmosphere research satellite (UARS) mission. *Journal of Geophysical Research*, *98*(D6), 10643–10647. https://doi.org/10.1029/92JD02828

Riley, W. J., Subin, Z. M., Lawrence, D. M., Swenson, S. C., Torn, M. S., Meng, L., et al. (2011). Barriers to predicting changes in global terrestrial methane fluxes: Analyses using CLM4Me. A methane biogeochemistry model integrated in CESM. *Biogeosciences*, *8*(7), 1925–1953. https://doi.org/10.5194/bg-8-1925-2011

Roche, A. E., Kumer, J. B., Mergenthaler, J. L., Ely, G. A., Uplinger, W. G., Potter, J. F., et al. (1993). The cryogenic limb array etalon spectrometer (CLAES) on UARS: Experiment description and performance. *Journal of Geophysical Research*, *98*(D6), 10763–10775. https://doi.org/10.1029/93JD00800

Rosentreter, J. A., Borges, A. V., Deemer, B. R., Holgerson, M. A., Liu, S., Song, C., et al. (2021). Half of global methane emissions come from highly variable aquatic ecosystem sources. *Nature Geoscience*, *14*(4), 225–230. https://doi.org/10.1038/s41561-021-00715-2

Rubino, M., Etheridge, D. M., Thornton, D. P., Howden, R., Allison, C. E., Francey, R. J., et al. (2019). Revised records of atmospheric trace gases CO_2, CH_4, N_2O, and $\delta^{13}C$-CO_2 over the last 2000 years from Law Dome, Antarctica. *Earth System Science Data*, *11*(2), 473–492. https://doi.org/10.5194/essd-11-473-2019

Russell, J. M., Gordley, L. L., Park, J. H., Drayson, S. R., Hesketh, W. D., Cicerone, R. J., et al. (1993). The halogen occultation experiment. *Journal of Geophysical Research*, *98*(D6), 10777–10797. https://doi.org/10.1029/93JD00799

Saunois, M., Bousquet, P., Poulter, B., Peregon, A., Ciais, P., Canadell, J. G., et al. (2016). The global methane budget 2000–2012. *Earth System Science Data*, *8*(2), 697–751. https://doi.org/10.5194/essd-8-697-2016

Saunois, M., Stavert, A. R., Poulter, B., Bousquet, P., Canadell, J. G., Jackson, R. B., et al. (2020). The global methane budget 2000–2017. *Earth System Science Data*, *12*(3), 1561–1623. https://doi.org/10.5194/essd-12-1561-2020

Schaefer, H. (2019). On the causes and consequences of recent trends in atmospheric methane. *Current Climate Change Reports*, *5*(4), 259–274. https://doi.org/10.1007/s40641-019-00140-z

Sellar, A. A., Jones, C. G., Mulcahy, J. P., Tang, Y., Yool, A., Wiltshire, A., et al. (2019). UKESM1: Description and evaluation of the U.K. Earth system model. *Journal of Advances in Modeling Earth Systems*, *11*(12), 4513–4558. https://doi.org/10.1029/2019MS001739

Sellar, A. A., Walton, J., Jones, C. G., Wood, R., Abraham, N. L., Andrejczuk, M., et al. (2020). Implementation of U.K. Earth system models for CMIP6. *Journal of Advances in Modeling Earth Systems*, *12*(4), e2019MS001946. https://doi.org/10.1029/2019MS001946

Shindell, D. T., Faluvegi, G., Stevenson, D. S., Krol, M. C., Emmons, L. K., Lamarque, J. F., et al. (2006). Multimodel simulations of carbon monoxide: Comparison with observations and projected near-future changes. *Journal of Geophysical Research*, *111*(D19), D19306. https://doi.org/10.1029/2006JD007100

Shindell, D. T., Pechony, O., Voulgarakis, A., Faluvegi, G., Nazarenko, L., Lamarque, J.-F., et al. (2013). Interactive ozone and methane chemistry in GISS-E2 historical and future climate simulations. *Atmospheric Chemistry and Physics*, *13*(5), 2653–2689. https://doi.org/10.5194/acp-13-2653-2013

Spivakovsky, C. M., Logan, J. A., Montzka, S. A., Balkanski, Y. J., Foreman-Fowler, M., Jones, D. B. A., et al. (2000). Three-dimensional climatological distribution of tropospheric OH: Update and evaluation. *Journal of Geophysical Research*, *105*(D7), 8931–8980. https://doi.org/10.1029/1999JD901006

Staniaszek, Z., Griffiths, P. T., Folberth, G. A., O'Connor, F. M., Abraham, N. L., & Archibald, A. T. (2022). The role of future anthropogenic methane emissions in air quality and climate. *npj Climate and Atmospheric Science*, *5*(1), 21. https://doi.org/10.1038/s41612-022-00247-5

Stein, O., Schultz, M. G., Bouarar, I., Clark, H., Huijnen, V., Gaudel, A., et al. (2014). On the wintertime low bias of Northern Hemisphere carbon monoxide found in global model simulations. *Atmospheric Chemistry and Physics*, *14*(17), 9295–9316. https://doi.org/10.5194/acp-14-9295-2014

Stevenson, D. S., Zhao, A., Naik, V., O'Connor, F. M., Tilmes, S., Zeng, G., et al. (2020). Trends in global tropospheric hydroxyl radical and methane lifetime since 1850 from AerChemMIP. *Atmospheric Chemistry and Physics*, *20*(21), 12905–12920. https://doi.org/10.5194/acp-20-12905-2020

Strode, S. A., Duncan, B. N., Yegorova, E. A., Kouatchou, J., Ziemke, J. R., & Douglass, A. R. (2015). Implications of carbon monoxide bias for methane lifetime and atmospheric composition in chemistry climate models. *Atmospheric Chemistry and Physics*, *15*(20), 11789–11805. https://doi.org/10.5194/acp-15-11789-2015

Strode, S. A., Worden, H. M., Damon, M., Douglass, A. R., Duncan, B. N., Emmons, L. K., et al. (2016). Interpreting space-based trends in carbon monoxide with multiple models. *Atmospheric Chemistry and Physics*, *16*(11), 7285–7294. https://doi.org/10.5194/acp-16-7285-2016

Szopa, S., Balkanski, Y., Schulz, M., Bekki, S., Cugnet, D., Fortems-Cheiney, A., et al. (2013). Aerosol and ozone changes as forcing for climate evolution between 1850 and 2100. *Climate Dynamics*, *40*(9-10), 2223–2250. https://doi.org/10.1007/s00382-012-1408-y

Szopa, S., Naik, V., Adhikary, B., Artaxo, P., Berntsen, T., Collins, W. D., et al. (2021). Short-lived climate forcers. In V. Masson-Delmotte, P. Zhai, A. Pirani, S.L. Connors, C. Péan, S. Berger, et al. (Eds.), *Climate Change 2021: The Physical Science Basis. Contribution of Working Group I to the Sixth Assessment Report of the Intergovernmental Panel on Climate Change* (pp. 817–922). Cambridge University Press. https://doi.org/10.1017/9781009157896.008

Tan, Z., & Zhuang, Q. (2015). Arctic lakes are continuous methane sources to the atmosphere under warming conditions. *Environmental Research Letters*, *10*(5), 054016. https://doi.org/10.1088/1748-9326/10/5/054016

Teixeira, J. C., Folberth, G. A., O'Connor, F. M., Unger, N., & Voulgarakis, A. (2021). Coupling interactive fire with atmospheric composition and climate in the UK Earth System Model. *Geoscientific Model Development*, *14*(10), 6515–6539. https://doi.org/10.5194/gmd-14-6515-2021

van Marle, M. J. E., Kloster, S., Magi, B. I., Marlon, J. R., Daniau, A.-L., Field, R. D., et al. (2017). Historic global biomass burning emissions for CMIP6 (BB4CMIP) based on merging satellite observations with proxies and fire models (1750–2015). *Geoscientific Model Development*, *10*(9), 3329–3357. https://doi.org/10.5194/gmd-10-3329-2017

von Schneidemesser, E., & Monks, P. S. (2013). Air quality and climate – synergies and trade-offs. *Air quality and climate - synergies and trade-offs, Environmental Science: Processes & Impacts*, *15*(7), 1315–1325. https://doi.org/10.1039/C3EM00178D

von Schneidemesser, E., Monks, P. S., Allan, J. D., Bruhwiler, L., Forster, P., Fowler, D., et al. (2015). Chemistry and the linkages between air quality and climate change. *Chemical Reviews*, *115*(10), 3856–3897. https://doi.org/10.1021/acs.chemrev.5b00089

Voulgarakis, A., Naik, V., Lamarque, J.-F., Shindell, D. T., Young, P. J., Prather, M. J., et al. (2013). Analysis of present day and future OH and methane lifetime in the ACCMIP simulations. *Atmospheric Chemistry and Physics*, *13*(5), 2563–2587. https://doi.org/10.5194/acp-13-2563-2013

Wild, O., Voulgarakis, A., O'Connor, F., Lamarque, J.-F., Ryan, E. M., & Lee, L. (2020). Global sensitivity analysis of chemistry–climate model budgets of tropospheric ozone and OH: Exploring model diversity. *Atmospheric Chemistry and Physics*, *20*(7), 4047–4058. https://doi.org/10.5194/acp-20-4047-2020

Williams, K. D., Copsey, D., Blockley, E. W., Bodas-Salcedo, A., Calvert, D., Comer, R., et al. (2018). The Met Office global Coupled-Model 3.0 and 3.1 (GC3.0 and GC3.1) configurations. *Journal of Advances in Modeling Earth Systems*, *10*(2), 357–380. https://doi.org/10.1002/2017MS001115

Wofsy, S. C., Afshar, S., Allen, H. M., Apel, E. C., Asher, E. C., Barletta, B., et al. (2021). ATom: Merged atmospheric chemistry, trace gases, and aerosols, version 2. *ORNL DAAC*. https://doi.org/10.3334/ORNLDAAC/1925

Yamazaki, K., Sexton, D. M. H., Rostron, J. W., McSweeney, C. F., Murphy, J. M., & Harris, G. R. (2021). A perturbed parameter ensemble of HadGEM3-GC3.05 coupled model projections: Part 2: Global performance and future changes. *Climate Dynamics*, *56*(11-12), 3437–3471. https://doi.org/10.1007/s00382-020-05608-5

Yool, A., Popova, E. E., & Anderson, T. R. (2013). MEDUSA-2.0: An intermediate complexity biogeochemical model of the marine carbon cycle for climate change and ocean acidification studies. *Geoscientific Model Development*, *6*(5), 1767–1811. https://doi.org/10.5194/gmd-6-1767-2013

Yvon-Durocher, G., Allen, A., Bastviken, D., Conrad, R., Gudasz, C., St-Pierre, A., et al. (2014). Methane fluxes show consistent temperature dependence across microbial to ecosystem scales. *Nature*, *507*(7493), 488–491. https://doi.org/10.1038/nature13164

Zhang, Z., Fluet-Chouinard, E., Jensen, K., McDonald, K., Hugelius, G., Gumbricht, T., et al. (2021). Development of the global data set of wetland area and dynamics for methane modeling (WAD2M). *Earth System Science Data*, *13*(5), 2001–2023. https://doi.org/10.5194/essd-13-2001-2021

Zhao, Y., Saunois, M., Bousquet, P., Lin, X., Berchet, A., Hegglin, M. I., et al. (2019). Inter-model comparison of global hydroxyl radical (OH) distributions and their impact on atmospheric methane over the 2000–2016 period. *Atmospheric Chemistry and Physics*, *19*(21), 13701–13723. https://doi.org/10.5194/acp-19-13701-2019